Drivetrain modelling of hybrid electric vehicles

Piotr Bera
AGH University of Science and Technology
al. Mickiewicza 30
30-059 Krakow
Poland
pbera@agh.edu.pl

Abstract

The aim of this paper is to present mathematical models of all the propulsion components of mild-hybrid and full-hybrid transmissions that allow the modelling process of fuel and energy consumption in any homologation driving cycle to be performed in detail. The characteristics provided in the article concern: the full load engine torque curve, full load electric motor power curve, combustion engine efficiency characteristic, including dynamic states and warm-up period, electric motor efficiency characteristic, inverter efficiency characteristic, battery characteristics in a wide temperature range and efficiency of the transmission. Moreover, the main principles concerning vehicle resistance and gear ratio selection are provided. The article concerns all the aspects limiting ranges of gear ratios, engine and motor(s) speed as well as their torque and power for the most common designs of hybrid transmissions: mild-hybrid with manual and dual-clutch gearbox, parallel full-hybrid with dual-clutch gearbox and full-hybrid e-CVT: series and series-parallel.

Keywords: hybrid transmission; brake specific fuel consumption; electric motor efficiency; gear ratio selection; battery efficiency

1. Introduction

The automotive industry is facing the difficult task of building cars with more powerful powertrains on the one hand, and using less fuel to meet the requirements imposed by the applicable standards on the other. Carbon dioxide (CO_2) emissions from road vehicles contribute to the greenhouse effect and are recognized as a gas of which emissions should be significantly reduced. EU regulations set CO_2 emission of passenger cars to 95 g/km in 2021 [1, 2]. Euro 7 [3, 4], which is planned to be introduced within a few years, will cut CO_2 as well as nitrogen oxide (NO_x), carbon oxide (CO) and particulate matter (PM) limits even more. This forces vehicle manufacturers to produce more efficient cars, which means: increasing the efficiency of the internal combustion engine (ICE) [5, 6], implementation of transmissions that use 7, 8 or 9 gears [7], vehicle weight reduction [8], improving aerodynamics [9] or rolling resistance reduction. In the future, clean transport will be based on battery electric vehicles (BEV) and fuel cell electric vehicles (FCEV) [10]. These vehicles are characterized by zero road emissions. However, for now, there are still many problems concerning both of these groups. In the case of BEVs, they concern: range anxiety [11], high price [12], performance at low temperature [13], battery durability [14], availability of rare earth elements [15] or black out problems [16] due to overloaded energy systems. In the case of FCEVs, problems concern mainly methods of hydrogen production, the small number of hydrogen stations, vehicle prices, the small market of such vehicles and policy issues [17]. Another way to decrease CO_2 emissions significantly is with hybrid electric vehicles (HEV), which refer to vehicles that use the ICE in conjunction with at least one electric motor (EM) and a high voltage traction battery (BAT) for propulsion. They are an area of interest of most

car manufacturers, because they combine the advantages of BEVs and ICE-only drivetrains: mature technology, affordable prices, no range anxiety, zero emission driving at low speed, high durability and reliability. Some car manufacturers already have most models available as HEVs. This is the reason for continuous development of simulation methods of such drivetrains.

The full analysis of a hybrid drivetrain is very complex because it involves a few overlapping areas: mechanical design including e.g. gearing, ICE and EM characteristics, BAT performance characteristics and optimization algorithms that join all the above components together. These areas involve the analysis of many variables, interactions, and non-linear characteristics, requiring multidisciplinary teams equipped with professional software to solve series of single problems. In [18], the authors introduced a novel architecture of a hybrid electric powertrain system, which lies between a series and a power-split and suppresses torque fluctuations and carries out the functionality of hybrid driving. In [19], the authors proposed a detailed analysis method to optimize the powertrain configuration of a single motor hybrid vehicle. The developed energy management strategy based on dynamic programming allowed the performance of the generated configurations to be analysed. Similar analysis, concerning the modelling and optimization techniques of four types of hybrid powertrain configurations available in the market, was conducted in [20]. In the case of dual clutch transmissions (DCT), gearshifts are the crucial moment when jerks may occur, thus sophisticated models are used to improve the driving comfort, fuel economy and drivetrain durability [21, 22]. In [23], the authors estimated the operating time share of electric and hybrid modes in real driving conditions (RDC) based on the electronically-controlled continuously variable transmission (e-CVT) series-parallel hybrid drivetrain. Analysis of the driver's operation allowed determination of the conditions of energy flow and the work share of the electric drive in the total driving time. In [24], the authors considered the influence of exploitation place on energy consumption, which is strongly connected with hybrid drivetrain programming and optimization. One element that significantly influences hybrid transmission functioning is the BAT. Its design influences size, efficiency and durability [10, 13, 14, 25÷29].

The purpose of this article is to provide all the necessary characteristics and coefficients that cover the whole working area of each component and allow a whole hybrid drivetrain to be modelled. To make models close to the real driving conditions, an ambient temperature range of -10÷40^{o}C, including ICE and BAT warm-up characteristics, ICE and EM dynamic states were considered. The presented models are created based on physical relationships, material properties, existing solutions, driving ergonomics and driving conditions based on the WLTP (Worldwide Harmonized Light-Duty Vehicles Test Procedure) homologation procedure. The formulas are a compromise between high accuracy and simplicity. All calculations are based on the data provided in the article.

The article is organized as follows: Section 2 describes the forces acting on a vehicle, Sections 3 and 4 describe the ICE and EM, respectively. Sections 5 and 6 describe inverter and BAT characteristics. Section 7 provides information concerning transmission losses, whereas Section 8 allows the inertia moment of rotating components to be calculated. Section 9 presents the criteria of maximum gear ratio and the ratio of maximum speed. Section 10 describes the most common designs of mild-hybrid and full-hybrid drivetrains and their specific design aspects with regard to the information presented in previous sections. Section 11 presents the conclusions.

2. Forces acting on a vehicle

A vehicle body is always subjected to external and internal forces that make it move or keep it at a standstill, which is presented in Fig. 1.

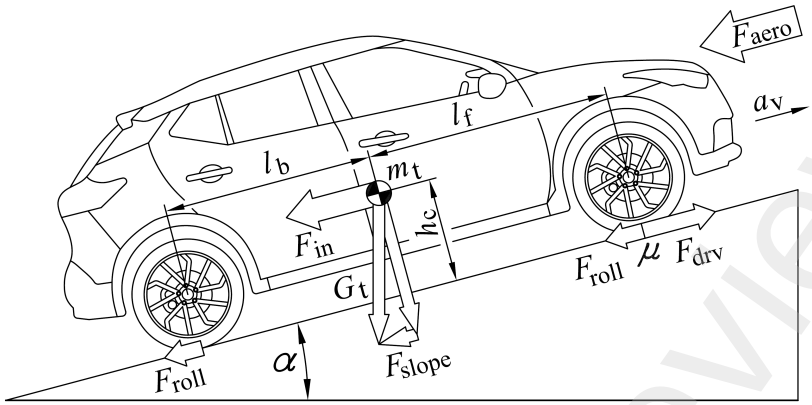

Fig. 1. Forces acting on a vehicle.

For a vehicle in motion, the driving force must overcome all resistances. According to the Newton laws, the acceleration of the vehicle a_v is:

$$a_v = \frac{F_{drv} - F_{roll} - F_{aero} - F_{slope}}{m_t \cdot \delta} \tag{1}$$

where m_t is the total vehicle mass, which is the sum of the empty vehicle mass m_e and actual load m_{load}, and cannot exceed the gross vehicle mass $m_{gross} \approx (1.3 \div 1.4) \cdot m_e$. The component δ is connected with rotating components of the vehicle, which generate additional resistance during vehicle acceleration. In a classic approach [30, 31, 32], where there is always a constant ratio between the ICE and wheels, this factor includes not only wheel inertia but also the ICE inertia J_{ICE} (including flywheel). In the case of hybrids, where the ICE (and generator GEN) might not be connected directly to the wheels by a constant transmission ratio, it is better to include the ICE and EM inertias in formulas (39) and (90). Coefficient δ includes only wheel and brake inertias. In initial calculations δ=1.04 can be assumed. The driving force F_{drv} comes from the ICE and/or EM and equals:

$$F_{drv} = \frac{M_{dyn} \cdot i_{gx} \cdot i_f \cdot \eta_{tr}}{R_d} \tag{2}$$

where M_{dyn} is a dynamic torque, including the ICE (39) and/or EM (90) inertia $J_{ICE/EM}$, i_{gx} is a gear ratio in the x^{th} gear and i_f is a gear ratio of the final drive (the product of $i_{gx} \cdot i_f = i_{tx}$ is the total transmission). A part of the power produced by the ICE or EM is lost due to the friction in the transmission. All losses in the transmission are represented by η_{tr} in formula (2). The dynamic wheel radius R_d takes into account the spring deflection of the tyre:

$$R_d = 0.485 \cdot D_w \tag{3}$$

where D_w is the free wheel diameter. The rolling resistance always resists the vehicle motion. It is mainly caused by hysteresis in the tyre material. The tyre rolling resistance force F_{roll} is:

$$F_{roll} = m_t \cdot g \cdot f_{roll}(p_{tyre}, v, G_t) \cdot \cos\alpha \tag{4}$$

where f_{roll} is the tyre rolling resistant coefficient, p_{tyre} [bar] is the tyre inflation pressure and $G_t = m_t \cdot g$ [N] is the total vehicle weight. The most precise f_{roll} formula for radial tyres is [33]:

$$f_{roll}(p_{tyre}, v, G_t) = 8 \cdot 10^{-4} \cdot \left[5.1 + \frac{5.5 \cdot 10^5 + 90 \cdot G_t}{p_{tyre} \cdot 10^5} + \frac{1100 + 0.0388 \cdot G_t}{p_{tyre} \cdot 10^5} \cdot \left(\frac{v}{3.6} \right)^2 \right] \tag{5}$$

Aerodynamic drag force in windless weather is expressed as:

$$F_{aero} = 0.5 \cdot \rho_{air} \cdot C_d \cdot A \cdot \left(\frac{v}{3.6} \right)^2 \tag{6}$$

Another external force that can either oppose forward motion of the vehicle or help it is the grading force:

$$F_{\text{slope}} = m_{\text{t}} \cdot g \cdot \sin\alpha \tag{7}$$

where α is the slope of the road. Road slope is limited by tyre friction (8) and for passenger cars cannot exceed 26%.

Formula (1) allows the theoretical vehicle acceleration a_{v} to be calculated. However, on a slippery road, in low gear or on an uphill road, the traction condition limits the vehicle acceleration a_{v}, thus the value calculated in (1) must be compared to the maximum possible acceleration $a_{\text{v}\mu}$:

$$a_{\text{v}\mu} = g \cdot \cos\alpha \cdot \left[\frac{\mu_{\text{f}} \cdot l_{\text{b}} + \mu_{\text{b}} \cdot l_{\text{f}}}{(l_{\text{b}} + l_{\text{f}}) + (\mu_{\text{f}} - \mu_{\text{b}}) \cdot h_{\text{c}}} - \text{tg}\alpha \right] \tag{8}$$

which takes into account the friction coefficient μ in the tyre-ground area, road slope α, vehicle mass distribution (l_{b}, l_{f}, h_{c}) and the drivetrain design: front-wheel drive (FWD), rear-wheel drive (RWD) or all-wheel drive (AWD). For FWD vehicles: $\mu_{\text{f}}=\mu$, $\mu_{\text{b}}=0$, for RWD: $\mu_{\text{b}}=\mu$, $\mu_{\text{f}}=0$, and for AWD vehicles: $\mu_{\text{b}}=\mu_{\text{f}}=\mu$. The desirable mass distribution is 50:50, however, in hybrids, due to a heavy drivetrain, the front axis may take up to 60% [34] of the load. The height of gravity centre h_{c}=0.4÷0.6 m.

3. Internal combustion engine

3.1. General description

The ICE converts the high density chemical energy of liquid fuel into mechanical energy. In full-hybrid transmissions naturally aspirated (NA) spark ignition (SI) Atkinson cycle ICEs are commonly used. They are characterized by a long piston stroke (the bore B to stroke S ratio, defined as $\gamma=B/S$, is in this case $\gamma\approx0.8$) and late intake valve closing. Mild-hybrid drivetrains are usually equipped with NA Otto ICEs or SI turbocharged (TB) ICEs. The ICE is characterized by the displacement V_{ICE}, nominal torque M_{M} developed at speed n_{M}, nominal power N_{N} developed at speed n_{N}, and [35] brake mean effective pressure *bmep* [MPa]:

$$bmep(n_{\text{M}}) = 0.01256 \cdot \frac{M_{\text{M}}}{V_{\text{ICE}}} \tag{9}$$

$$bmep(n_{\text{N}}) = 120 \cdot \frac{N_{\text{N}}}{n_{\text{N}} \cdot V_{\text{ICE}}} = C_{\text{NM}} \cdot bmep(n_{\text{M}}) \tag{10}$$

The parameters allowing (9)÷(11) and (21) to be defined are presented in Table 1.

Table 1
Parameters of SI ICEs used in mild-hybrid and full-hybrid transmissions.

No	Parameter	SI NA Atkinson	SI NA Otto	SI TB Otto	SI Miller (charged)
1	$bmep(n_{\text{M}})$ [MPa]	1.0÷1.1	1.2÷1.3	1.8÷2.5	1.5÷1.8
2	n_{M} [rpm]	3000÷4000	3500÷5000	1400÷2500	1400÷4400
3	n_{N} [rpm]	5000÷5700	5000÷6300	4500÷6000	5000÷5500
4	C_{NM} [-]*	0.80÷0.95	0.70÷0.90	0.70÷0.90	0.85÷0.90
5	CR [-]	13.0÷14.0	10.8_{MPI} ÷ 11.0_{GDI}	10.0_{MPI} ÷10.5_{GDI}	<12.5
6	η_{max} [%]	41	38	36	38
7	$M(\text{P}_0)$ [Nm]	$(0.8\div0.9)\cdot M_{\text{M}}$	$(0.7\div0.8)\cdot M_{\text{M}}$	$(0.6\div0.7)\cdot M_{\text{M}}$	$(0.7\div0.8)\cdot M_{\text{M}}$
8	$M(\text{P}_1)$ [Nm]	$\sim0.15\cdot M_{\text{M}}$	$\sim0.15\cdot M_{\text{M}}$	$\sim0.15\cdot M_{\text{M}}$	$\sim0.15\cdot M_{\text{M}}$
9	$g_{\text{e}}(\text{P}_1)$ [g/kWh]	$\sim1.7\cdot g_{\text{e}}(\text{P}_0)$	$\sim1.8\cdot g_{\text{e}}(\text{P}_0)$	$\sim1.4\cdot g_{\text{e}}(\text{P}_0)$	$\sim1.4\cdot g_{\text{e}}(\text{P}_0)$

*smaller value for greater n_{N}, greater value for smaller n_{N} and when $bmep(n_{\text{M}})$ is small, CR – compression ratio, MPI – multi point port injection, GDI – gasoline direct injection, points: 6÷9 – see Fig. 3, $\eta_{\text{max}} = \eta(\text{P}_0)$

Points 6÷9 in Table 1 concern the brake specific fuel consumption (*bsfc*) characteristic (described later in Section 3.3) and represent average values for particular ICE design.

3.2. ICE torque and power characteristics

The ICE power N and torque M characteristics versus rotational speed n with the throttle fully opened (Fig. 2) are based on 5 points marked with solid dots. Torque M_N (hollow dot) is not given in the technical data but can be calculated based on n_N and N_N (17).

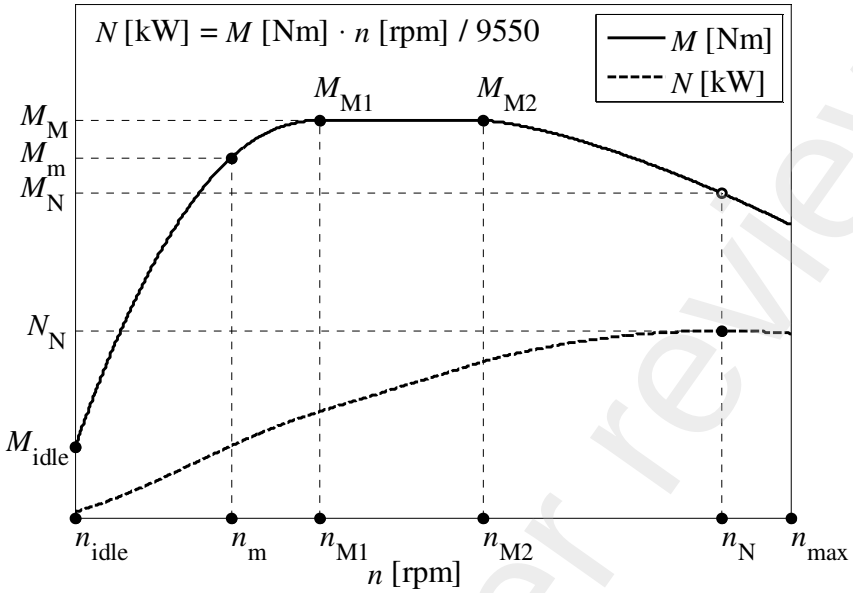

Fig. 2. ICE power and torque performance curves.

The following formula can be used both for ICEs where the peak torque M_M occurs at one speed as well as in a wide speed range ($n_{M1} \div n_{M2}$):

$$M(n) = -a_0 \cdot |n - n_0|^p + M_M \tag{11}$$

where the coefficients depending on n are:

$$n_0 = \frac{n_{M2} - n_{M1}}{1 + 0.5\text{^}[n - 0.5 \cdot (n_{M1} + n_{M2})]} + n_{M1} \tag{12}$$

$$a_0 = \left[\frac{-a_1}{1 + 0.01\text{^}(n - n_{M1})} + a_1 + \frac{a_2}{1 + 0.01\text{^}(n - n_{M2})} \right] \tag{13}$$

$$p = \frac{p_2 - p_1}{1 + 0.5\text{^}[n - 0.5 \cdot (n_{M1} + n_{M2})]} + p_1 \tag{14}$$

and the constants:

$$p_1 = \frac{\ln[(M_m - M_M)/(M_{idle} - M_M)]}{\ln[(n_{M1} - n_m)/(n_{M1} - n_{idle})]} \tag{15}$$

$$a_1 = \frac{M_M - M_{idle}}{(n_{M1} - n_{idle})\text{^}p_1} \tag{16}$$

$$M_N = 9550 \cdot N_N / n_N \tag{17}$$

$$p_2 = \frac{M_N \cdot (n_N - n_{M2})}{n_N \cdot (M_M - M_N)} \tag{18}$$

$$a_2 = \frac{M_M - M_N}{(n_N - n_{M2})\text{^}p_2} \tag{19}$$

The range above n_N is rarely used, thus formula (11) allows this range to be approximated from the previous range with reasonable accuracy.

3.3. Brake specific fuel consumption characteristic

The overall efficiency η_{ICE} reaches over 40% for SI Atkinson cycle ICEs commonly used in full-hybrid drivetrains. This parameter is sometimes presented in the form of η_{ICE} contours in a coordinate system of n and M. It can also be presented as a *bsfc* characteristic (Fig. 3).

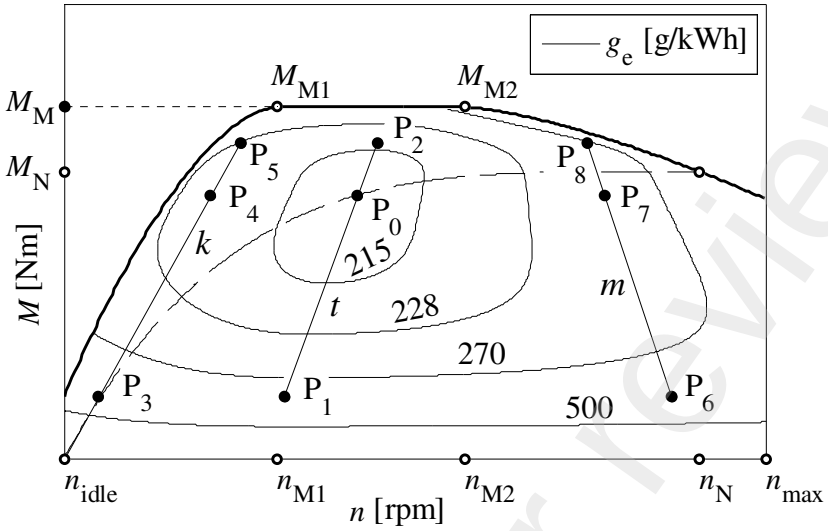

Fig. 3. *Bsfc* characteristic.

The η_{ICE} and *bsfc* can be used interchangeably (petrol calorific value W_p=43 MJ/kg [35]):

$$\eta_{ICE} = \frac{84}{g_e} \cdot 100\% \tag{20}$$

To obtain such a characteristic (21), one should provide g_e (η_{ICE}), n and M for 9 points: $P_0 \ldots P_8$. Specific conditions are: $M_{P0}=M_{P4}=M_{P7}$, $M_{P1}=M_{P3}=M_{P6}$ and $M_{P2}=M_{P5}=M_{P8}$. Maximum efficiency η_{max} is reached at P_0. The dashed line represents the optimum operating curve. The formula for η_{ICE} in the whole working range is the following:

$$\eta_{ICE} = -\left[\frac{(\eta_t - \eta_m)/(n_t - n_m)^2 - (\eta_t - \eta_k)/(n_t - n_k)^2}{1 + 0.01\text{^}(n - n_t)} + \frac{\eta_t - \eta_k}{(n_t - n_k)^2}\right] \cdot (n - n_t)^2 + \eta_t \tag{21}$$

where the variables depending on the torque M are:

$$\eta_k = \left[\frac{a_{kd} - a_{kg}}{1 + 0.01\text{^}(M - M_{P4})} - a_{kd}\right] \cdot |M - M_{P4}|\text{^}\, p_k + \eta_{P4} \tag{22}$$

$$n_k = M \cdot \frac{n_{P4} - n_{idle}}{M_{P4}} + n_{idle} \tag{23}$$

$$\eta_t = \left[\frac{a_{td} - a_{tg}}{1 + 0.01\text{^}(M - M_{P0})} - a_{td}\right] \cdot |M - M_{P0}|\text{^}\, p_t + \eta_{P0} \tag{24}$$

$$n_t = (M - M_{P1}) \cdot \frac{n_{P0} - n_{P1}}{M_{P0} - M_{P1}} + n_{P1} \tag{25}$$

$$\eta_m = \left[\frac{a_{md} - a_{mg}}{1 + 0.01\text{^}(M - M_{P7})} - a_{md}\right] \cdot |M - M_{P7}|\text{^}\, p_m + \eta_{P7} \tag{26}$$

$$n_m = (M - M_{P6}) \cdot \frac{n_{P7} - n_{P6}}{M_{P7} - M_{P6}} + n_{P6} \tag{27}$$

the constant values connected with line k:

$$p_k = \frac{\ln[(\eta_{P4} - \eta_{P3})/\eta_{P4}]}{\ln[(M_{P4} - M_{P3})/M_{P4}]} \tag{28}$$

$$a_{\mathrm{kd}} = \eta_{\mathrm{P4}} / \left(M_{\mathrm{P4}} \wedge p_{\mathrm{k}}\right) \tag{29}$$

$$a_{\mathrm{kg}} = \frac{\eta_{\mathrm{P4}} - \eta_{\mathrm{P5}}}{\left(M_{\mathrm{P5}} - M_{\mathrm{P4}}\right) \wedge p_{\mathrm{k}}} \tag{30}$$

the constant values connected with line *t*:

$$p_{\mathrm{t}} = \frac{\ln\left[\left(\eta_{\mathrm{P0}} - \eta_{\mathrm{P1}}\right)/\eta_{\mathrm{P0}}\right]}{\ln\left[\left(M_{\mathrm{P0}} - M_{\mathrm{P1}}\right)/M_{\mathrm{P0}}\right]} \tag{31}$$

$$a_{\mathrm{td}} = \eta_{\mathrm{P0}} / \left(M_{\mathrm{P0}} \wedge p_{\mathrm{t}}\right) \tag{32}$$

$$a_{\mathrm{tg}} = \frac{\eta_{\mathrm{P0}} - \eta_{\mathrm{P2}}}{\left(M_{\mathrm{P2}} - M_{\mathrm{P0}}\right) \wedge p_{\mathrm{t}}} \tag{33}$$

and the constant values connected with line *m*:

$$p_{\mathrm{m}} = \frac{\ln\left[\left(\eta_{\mathrm{P7}} - \eta_{\mathrm{P6}}\right)/\eta_{\mathrm{P7}}\right]}{\ln\left[\left(M_{\mathrm{P7}} - M_{\mathrm{P6}}\right)/M_{\mathrm{P7}}\right]} \tag{34}$$

$$a_{\mathrm{md}} = \eta_{\mathrm{P7}} / \left(M_{\mathrm{P7}} \wedge p_{\mathrm{m}}\right) \tag{35}$$

$$a_{\mathrm{mg}} = \frac{\eta_{\mathrm{P7}} - \eta_{\mathrm{P8}}}{\left(M_{\mathrm{P8}} - M_{\mathrm{P7}}\right) \wedge p_{\mathrm{m}}} \tag{36}$$

The above characteristic allows the calculation of a *bsfc* in steady states (when *n* and *M* are constant) and at a nominal working temperature, which is usually about 90°C.

Formula (37) allows the mileage fuel consumption G_{V} [dm^3/100 km] for a constant *v*, also during the warm-up period (the ICE temperature influences the equivalence ratio $\lambda(temp_{\mathrm{ICE}})$ (63) and oil viscosity influences friction torque (39), (57)), to be calculated:

$$G_{\mathrm{v}} = 1.05 \cdot \frac{g_{\mathrm{e}}\left(n, M_{\mathrm{dyn}}\right)}{\lambda\left(temp_{\mathrm{ICE}}\right)} \cdot \frac{M_{\mathrm{dyn}} \cdot n}{v \cdot \rho_{\mathrm{fuel}}} \cdot 10^{-5} \tag{37}$$

The idle consumption G_{h} [dm^3/h] needs a small torque to be assumed, e.g. M_{dyn}=0.1 Nm (at M=0 g_{e} cannot be calculated). Then the formula is:

$$G_{\mathrm{h}} = 1.05 \cdot \frac{g_{\mathrm{e}}\left(n_{\mathrm{idle}}, M_{\mathrm{dyn}}\right)}{\lambda\left(temp_{\mathrm{ICE}}\right)} \cdot \frac{M_{\mathrm{dyn}} \cdot n_{\mathrm{idle}}}{\rho_{\mathrm{fuel}}} \cdot 10^{-7} \tag{38}$$

Sections 3.4, 3.5 and 3.6 allow characteristics to be obtained which can also be used at dynamic states, during the warm-up period and at ICE start-up, respectively.

3.4. Dynamic states

Detailed models, based on artificial neural networks, can be used [36, 37] to represent dynamic behaviour of the ICE, however, they require plenty of detailed data concerning the particular ICE. Thus, the following model of ICE behaviour in dynamic states can be used:

$$M_{\mathrm{dyn}} = M - M_{\mathrm{fr\_}\nu} - J_{\mathrm{ICE}} \cdot \varepsilon_{\mathrm{ICE}} \cdot \left[1 + k_{\mathrm{nm}} \cdot \mathrm{sgn}\left(\varepsilon_{\mathrm{ICE}}\right)\right] \tag{39}$$

where the ICE inertia J_{ICE} (including flywheel) is [38, 39]:

$$J_{\mathrm{ICE}} = 0.1 \cdot \left(V_{\mathrm{ICE}}^2 - V_{\mathrm{ICE}} + 1\right) \tag{40}$$

The coefficient k_{nm}<0.05 takes into account non-mechanical inertias of the oil and coolant. $M_{\mathrm{fr\_v}}$ is the friction torque (57) generated by the oil when $temp_{\mathrm{oil}}$<100°C.

3.5. Warm-up period

When a cold ICE starts at an ambient temperature $temp_{\mathrm{amb}}$ it consumes much more fuel than at a nominal working temperature because of the increased oil viscosity and air-fuel mixture enrichment. Determination of heat phenomena during the warm-up time is important in overall fuel consumption analysis and has been investigated in many research projects [40÷46]. However, heat processes in an ICE are very complex due to the fact that heat and cooling sources occur in different areas and have different thermal properties: temperature,

specific heat C [J/(kgK)] and heat transfer coefficient h [W/(m^{2}K)]. Several assumptions are made to simplify the ICE thermal model, simultaneously keeping it close to real phenomena:
- ICE temperature is represented by a coolant temperature ($temp_{ICE}$= $temp_{clnt}$),
- formula for ICE temperature increase is valid for $temp_{ICE}$<90^{o}C (then heat transfer is controlled by a thermostat and radiator so $temp_{ICE}$≈const.),
- the pistons, cylinders, cylinder head and oil pan are made of aluminium, while the crankshaft and connecting rods are made of steel,
- pistons are cooled only by an oil mist from crankshaft bearings (piston jet cooling or through a gallery in the piston is not included),
- dimensions of ICE elements [35] are proportional to V_{ICE}.

All the heat H_{IN} generated in SI ICE has its source in a combustion process [35, 40]. With regard to W_p it results in:

$$H_{IN} = 12 \cdot g_e \cdot N_{ICE} \tag{41}$$

In nominal working conditions, part of H_{IN} is transferred to a cooling system [35, 40, 47]:

$$H_{cool} = 1.33 \cdot n^{0.46} \cdot H_{IN}^{0.51} \tag{42}$$

which is 15÷40% of total heat (41) delivered to the ICE. In the warm-up period, this heat accumulates in the pistons, block, head and coolant in a small circuit (including a cabin heat exchanger). The coolant volume in a small circuit is k_{sc}≈30% of total coolant volume. Part of H_{cool} is transferred from the coolant to the cabin heat exchanger:

$$H_{che} = 10^{-3} \cdot h_{che} \cdot V_{che} \cdot \beta_{che} \cdot (temp_{clnt} - temp_{amb}) \tag{43}$$

This heat depends on fan speed and is defined by a variable *lev*.=0, 1…4 (Table 3).

Heat is also given away to the surroundings through the cylinder block and head, cooled by the air flowing by:

$$H_{bh} = A_{bh} \cdot h_{bh} \cdot (temp_{clnt} - temp_{amb}) \tag{44}$$

The area A_{bh} (Table 3) includes the area of ribs which increase the heat transfer area.

Part of H_{cool} is transferred to the oil in the heat exchanger H_{hex}, which usually has a plate type design (the distance between plates is ~3.5 mm). Heat flow from the coolant to the oil is:

$$H_{hex} = 10^{-3} \cdot h_{hex} \cdot V_{hex} \cdot \beta_{hex} \cdot (temp_{clnt} - temp_{oil}) \tag{45}$$

Oil is also warmed-up by contact with hot ICE parts. This heat depends on the total oil pump flow Q_{oil} [kg/s] in the ICE [35, 48÷51], which can be described by the following model:

$$Q_{oil} = 9.2 \cdot 10^{-11} \cdot N_N \cdot (n / n_N)^{0.625} \cdot (temp_{oil} + 50)^{3.5} \tag{46}$$

By means of splash lubrication, part of the total input heat (<15%·H_{IN}) [49, 52÷56] is transferred to an oil mist in a crankcase:

$$H_{mist} = C_{oil} \cdot k_{cyl} \cdot Q_{oil} \cdot [temp_{ICE} + (10 + 50 \cdot N / N_N) - temp_{oil}] \tag{47}$$

where k_{cyl}≈0.2 is the part of total flow (46) that creates the oil mist lubricating cylinder walls and pistons. Another part of heat is transferred from the ICE block to the oil when it is in the valve-train area and then flows down to the oil pan:

$$H_{cam} = C_{oil} \cdot k_{cam} \cdot Q_{oil} \cdot (temp_{ICE} - temp_{oil}) \tag{48}$$

where k_{cam}≈0.02 determines the fraction of Q_{oil} to the valve-train [49]. The heat that the oil transfers through the oil pan to the air increases with vehicle speed and is:

$$H_{pan} = A_{pan} \cdot h_{pan} \cdot (temp_{oil} - temp_{amb}) \tag{49}$$

Moreover, part of the total heat H_{IN} (41) is used to overcome friction, which generates the heat. This is an important part of energy loss (mainly in the area of crankshaft bearings and piston-cylinder assembly), which plays an important role in ICE warm-up, and generates additional resistance torque included in the total resistance torque (39). It can be calculated precisely according to the Patton friction model and further modifications [57, 58]. Three characteristics of the most common oils are presented in Table 2.

Table 2
Specifications of 0W-16, 0W-20 and 5W-30 oils.

Oil	$\nu(40^{\circ}C)$ [mm^2/s]	$\nu(100^{\circ}C)$ [mm^2/s]	k_{oil} [mm^2/s]	Θ_1 [$^{\circ}$C]	Θ_2 [$^{\circ}$C]
0W-16	29.9	6.7	0.125	871.9	119.7
0W-20	44.9	8.6	0.129	889.6	112.5
5W-30	66.4	11.7	0.088	1116	129.0
$\nu(temp_{oil})=k_{oil}\cdot\exp[\theta_1/(\theta_2+temp_{oil})]$					

All the *fmep* [kPa] factors [57], connected with mechanical friction phenomena in the area of the crankshaft ($_{crk}$), pistons ($_{pst}$) and camshafts ($_{cam}$), are the following:

$$fmep_{total}=\sqrt{\frac{\nu(temp_{oil})}{\nu(100^{\circ}C)}}\cdot[fmep_{crk1}(\nu)+fmep_{pst1}(\nu)+fmep_{cam1}(\nu)]+[fmep_{crk2}+fmep_{pst2}+fmep_{cam2}] \quad (50)$$

where:

$$fmep_{crk1}(\nu)=3.03\cdot10^{-4}\cdot n\cdot B\cdot\gamma\cdot\left(0.129\cdot\frac{n_c+1}{n_c}+0.096\right) \quad (51)$$

$$fmep_{crk2}=0.85\cdot10^{5}\cdot\frac{\gamma}{B^2\cdot n_c}+0.66\cdot10^{-10}\cdot\frac{B^2\cdot n^2\cdot(n_c+1)}{n_c} \quad (52)$$

$$fmep_{pst1}(\nu)=0.0098\cdot\frac{n}{\gamma}+4\cdot\frac{M\cdot bmep(n_M)}{M(n)}+2.07 \quad (53)$$

$$fmep_{pst2}=\frac{3.66\cdot10^{4}}{B^2}\cdot\left(1+\frac{500}{n}\right)+\left(0.7\cdot bmep(n_M)\cdot\frac{M}{M(n)}+0.36\right)\cdot\left[CR\text{^}\left(1.33-\frac{9.33\cdot n\cdot B}{10^{7}\cdot\gamma}\right)\right] \quad (54)$$

$$fmep_{cam1}(\nu)=84\cdot\left[5.08\cdot\frac{n\cdot(n_c+2)\cdot\gamma}{B^3\cdot n_c}+\frac{\sqrt{n}\cdot\gamma}{B^2}\right] \quad (55)$$

where CR is the effective compression ratio and n_c is the number of cylinders. The cylinder bore B [mm], can be calculated in the following way:

$$B=108.4\cdot\sqrt[3]{\gamma\cdot V_{ICE}/n_c} \quad (56)$$

The factor $fmep_{cam2}$ including friction factors connected with valve-train design independent of oil viscosity can be ignored, because it is small, and it is difficult to differentiate the heat from the valve-train from combustion heat.

The *bsfc* characteristic (Fig. 3) includes oil friction when the ICE and oil have nominal working temperatures. Thus, to calculate fuel consumption (37)÷(38) and dynamics (39) at lower oil temperature, only factors dependent on oil viscosity are considered:

$$M_{fr\_\nu}=\frac{V_{ICE}}{12.56}\cdot\left\{\sqrt{\frac{k_{oil}\cdot\exp[\theta_1/(\theta_2+temp_{oil})]}{\nu(100^{\circ}C)}}-1\right\}\cdot\left[fmep_{crk1}(\nu)+fmep_{pst1}(\nu)+fmep_{cam1}(\nu)\right] \quad (57)$$

However, in the case of calculations of heat transfer, it is the total piston friction H_{fr_pst} which warms up the coolant:

$$H_{fr\_pst}=\frac{V_{ICE}\cdot n}{120}\cdot\left\{\sqrt{\frac{k_{oil}\cdot\exp[\theta_1/(\theta_2+temp_{oil})]}{\nu(100^{\circ}C)}}\cdot fmep_{pst1}(\nu)+fmep_{pst2}\right\} \quad (58)$$

and the total crankshaft friction H_{fr_crk} which warms up the oil:

$$H_{fr\_crk}=\frac{V_{ICE}\cdot n}{120}\cdot\left\{\sqrt{\frac{k_{oil}\cdot\exp[\theta_1/(\theta_2+temp_{oil})]}{\nu(100^{\circ}C)}}\cdot fmep_{crk1}(\nu)+fmep_{crk2}\right\} \quad (59)$$

Fig. 4 presents an example of the friction torque in a wide range of oil temperature.

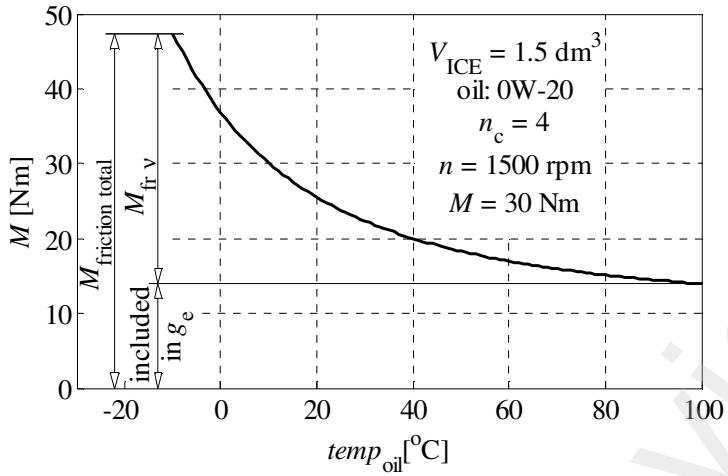

Fig. 4. ICE friction torque vs oil temperature.

The heat transfer between different parts of the ICE depends on their areas A, which are the function of B (56), and masses (Table 3), which are proportional to the total ICE mass:

$$m_{\mathrm{ICE}} = (40 \cdot V_{\mathrm{ICE}} + 35) \cdot k_{\mathrm{ICE}} \tag{60}$$

where k_{ICE}=1.0 for NA ICE and k_{ICE}=1.2 for charged ICE. Table 3 presents the specifications of materials and elements required for ICE warm-up calculations.

Table 3
Specifications of ICE materials and parts (average values).

Part name ($_{\mathrm{abbr.}}$)	ρ [kg/m^3]	V [dm^3]	m [kg]	A [m^2]	C [J/(kgK)]	β [m^2/m^3]	h [W/(m^{2}K)]
oil ($_{\mathrm{oil}}$)	850	4÷5	$10^{-3}\cdot\rho_{\mathrm{oil}}\cdot V_{\mathrm{oil}}$	-	1985	-	-
coolant ($_{\mathrm{clnt}}$)	1070	5÷9	$10^{-3}\cdot\rho_{\mathrm{clnt}}\cdot V_{\mathrm{clnt}}$	-	3300	-	-
cabin heat exch.[1] ($_{\mathrm{che}}$)	2700	1.0÷1.8	-	-	930	1000	$5\cdot(lev.+1)$
oil heat exch.[1] ($_{\mathrm{hex}}$)	2700	$0.3\cdot V_{\mathrm{ICE}}$	-	-	930	600	300
block, head[1] ($_{\mathrm{bh}}$)	2700	-	$25\%\cdot m_{\mathrm{ICE}}$	$2\cdot10^{-5}\cdot n_c\cdot B^2$	930	-	$5+12\cdot v^{0.25}$
pistons[1] ($_{\mathrm{pst}}$)	2700	-	$1.2\%\cdot m_{\mathrm{ICE}}$	-	930	-	-
oil pan[1] ($_{\mathrm{pan}}$)	2700	-	$2\%\cdot m_{\mathrm{ICE}}$	$9\cdot10^{-6}\cdot n_c\cdot B^2$	930	-	$5+12\cdot v^{0.25}$
crankshaft[2] ($_{\mathrm{crk}}$)	8750	-	$12\%\cdot m_{\mathrm{ICE}}$	-	490	-	50

[1]made of aluminium, [2]made of steel

Taking the above into consideration, the oil temperature changes according to:

$$\Delta temp_{\mathrm{oil}} = \frac{H_{\mathrm{mist}} + H_{\mathrm{fr\_crk}} + H_{\mathrm{hex}} + H_{\mathrm{cam}} - H_{\mathrm{pan}}}{C_{\mathrm{oil}} \cdot \rho_{\mathrm{oil}} \cdot V_{\mathrm{oil}} + k_{\mathrm{add}} \cdot C_{\mathrm{crk}} \cdot m_{\mathrm{crk}} + C_{\mathrm{pan}} \cdot m_{\mathrm{pan}}} \cdot \Delta t \tag{61}$$

where k_{add}=1.2 includes additional mass of the crankshaft support. The ICE temperature change in the time interval Δt is:

$$\Delta temp_{\mathrm{ICE}} = \frac{H_{\mathrm{cool}} + H_{\mathrm{fr\_pst}} - H_{\mathrm{che}} - H_{\mathrm{mist}} - H_{\mathrm{bh}} - H_{\mathrm{hex}}}{C_{\mathrm{bh}} \cdot m_{\mathrm{bh}} + C_{\mathrm{pst}} \cdot m_{\mathrm{pst}} + k_{\mathrm{sc}} \cdot C_{\mathrm{clnt}} \cdot \rho_{\mathrm{clnt}} \cdot V_{\mathrm{clnt}}} \cdot \Delta t \tag{62}$$

The equivalence ratio λ during the warm-up period depends on $temp_{\mathrm{ICE}}$ and is:

$$\lambda(temp_{\mathrm{ICE}}) = \left[1.7 - \frac{0.7}{1 + \exp(-0.08 \cdot temp_{\mathrm{ICE}})}\right]^{-1} \tag{63}$$

An example of oil and coolant warm-up in the WLTP test (B-class vehicle, parallel hybrid, m_{t}=1250 kg, V_{ICE}=1.0 dm^3, N_{N}=75 kW, V_{oil}=4 dm^3 and V_{clnt}=5 dm^3), based on the above relationships, is presented in Fig. 5.

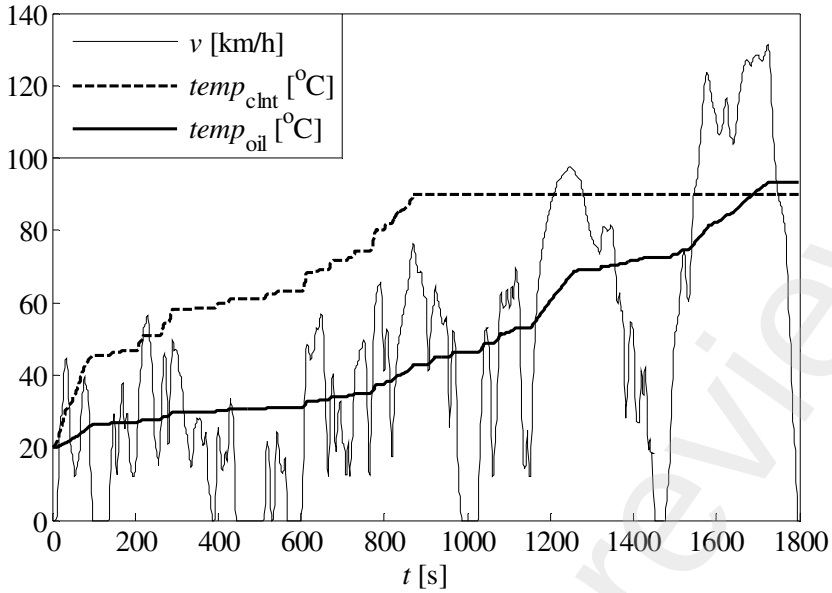

Fig. 5. Coolant and oil temperature in the WLTP test.

After ICE start-up at an ambient temperature, it usually works permanently until it reaches at least ~40°C. Then a stop-start function is activated.

3.6. ICE start

In a hybrid transmission, the ICE is permanently stopped and started. A quick response to provide an immediate reaction to the driver demands results in a high angular acceleration of the EM and ICE connected together by means of a gear pair, planetary gear, multirib v-belt or directly, depending on the hybridization level and transmission design. The gear ratio between the EM and ICE is:

$$i_{\mathrm{EM\_ICE}} = \frac{n_{\mathrm{EM}}}{n_{\mathrm{ICE}}} = \frac{n_{\mathrm{EM\_start}}}{n_{\mathrm{ICE\_start}}} = \frac{\varepsilon_{\mathrm{EM}}}{\varepsilon_{\mathrm{ICE}}} = (1.000 \div 2.500) \tag{64}$$

The efficiency of this connection is $\eta_{\mathrm{EM\_ICE}}$=(0.95÷1.00). When the ICE is stopped, the EM acts as a starter and uses electric energy supplied from the BAT to put the ICE into motion. In the ICE start process, the EM must overcome its own inertia (90) and ICE resistances: inside friction, inertia, pressure loading and pumping losses. To ensure a quick and smooth start, the ICE must reach $n_{\mathrm{ICE\_start}}$≈1000 rpm in about 250 ms [61, 62], which results in an angular acceleration of $\varepsilon_{\mathrm{ICE}}$≈400 rad/s^2. Again, the friction model [57, 58] is used. This time, it includes pumping losses in the intake manifold and constant friction members. It is used with the same assumptions concerning ICE design, which results in:

$$M_{\mathrm{ICE\_start}} = J_{\mathrm{ICE}} \cdot \varepsilon_{\mathrm{ICE}} + k_{\mathrm{start}} \cdot V_{\mathrm{ICE}} \tag{65}$$

where k_{start} is:

$$k_{\mathrm{start}} = \nu(100^{\mathrm{o}}\mathrm{C}) \cdot \left(0.965\text{^}temp_{\mathrm{oil}}\right) + 12.2 \tag{66}$$

The coefficient k_{start} varies significantly with oil temperature, e.g. for 5W-30 oil: k_{start}=(28, 12) for (-10°C, 90°C) respectively. From $M_{\mathrm{ICE\_start}}$ calculated in (65) one can determine the peak power at the ICE start process:

$$N_{\mathrm{ICE\_start}} = \frac{M_{\mathrm{ICE\_start}} \cdot n_{\mathrm{ICE\_start}}}{9550} \tag{67}$$

Due to the fact that in a full-hybrid transmission the ICE might be off up to 80% of city driving time, the ICE oil temperature is low for a long time from start-up. Thus, $M_{\mathrm{ICE\_start}}$ (65) should be calculated for the oil temperature of ~20÷30°C.

4. Electric motor

4.1. Electric motor torque characteristic

EM is a better propulsion for automotive vehicles than the ICE due to its numerous advantages: small size (high power and torque density), perfect balance, high speed range (in automotive applications they reach a maximum speed of ~15 000 rpm [34]), high torque from zero speed and high efficiency (over 97% [34]) in a wide range of work field. It provides constant torque in the initial speed range and constant power in the second range, which is presented in Fig. 6.

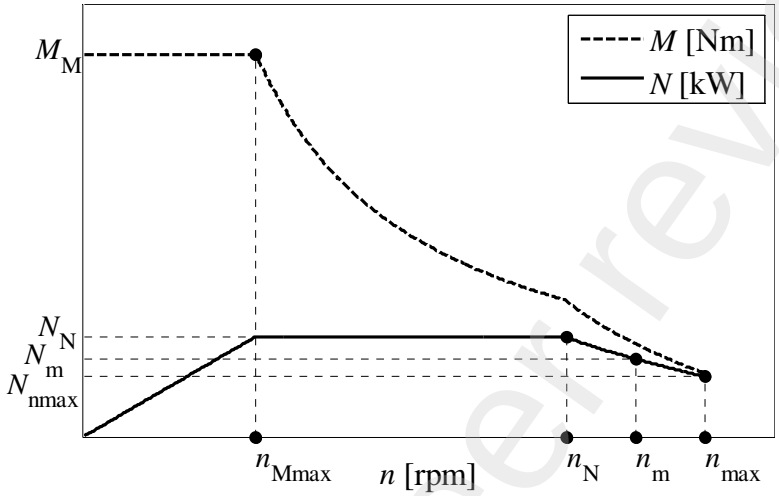

Fig. 6. EM power and torque characteristics.

It is used to propel the vehicle or/and works as ICE starter/generator. From the rated speed n_{Mmax}:

$$n_{\mathrm{M\,max}} = 9550 \cdot \frac{N_{\mathrm{N\_EM}}}{M_{\mathrm{M\_EM}}} \tag{68}$$

the torque changes with a hyperbolic relationship to the speed n_{N}, and further in the natural mode region, torque decreases proportionally to the square of the speed [34]. To draw graphs of N and M (Fig. 6) specific parameters for given points (solid dots) must be provided.

The following formula can be used to calculate N in the whole range of n:

$$N(n) = -a_0 \cdot \left| n - n_0 \right|^p + N_{\mathrm{N}} \tag{69}$$

where the variables are the following:

$$n_0 = \frac{n_{\mathrm{N}} - n_{\mathrm{Mmax}}}{1 + 0.5\text{^}\left[n - 0.5 \cdot \left(n_{\mathrm{Mmax}} + n_{\mathrm{N}} \right) \right]} + n_{\mathrm{Mmax}} \tag{70}$$

$$a_0 = \left[\frac{-N_{\mathrm{N}} / n_{\mathrm{M\,max}}}{1 + 0.01\text{^}\left(n - n_{\mathrm{Mmax}} \right)} + \frac{N_{\mathrm{N}}}{n_{\mathrm{M\,max}}} + \frac{a_2}{1 + 0.01\text{^}\left(n - n_{\mathrm{N}} \right)} \right] \tag{71}$$

$$p = \frac{p_2 - 1}{1 + 0.5\text{^}\left[n - 0.5 \cdot \left(n_{\mathrm{Mmax}} + n_{\mathrm{N}} \right) \right]} + 1 \tag{72}$$

and the constants:

$$p_2 = \frac{\ln\left[\left(N_{\mathrm{N}} - N_{\mathrm{nmax}} \right) / \left(N_{\mathrm{N}} - N_{\mathrm{m}} \right) \right]}{\ln\left[\left(n_{\mathrm{max}} - n_{\mathrm{N}} \right) / \left(n_{\mathrm{m}} - n_{\mathrm{N}} \right) \right]} \tag{73}$$

$$a_2 = \frac{N_{\mathrm{N}} - N_{\mathrm{m}}}{\left(n_{\mathrm{m}} - n_{\mathrm{N}} \right)\text{^}\, p_2} \tag{74}$$

The above formula can be used in calculations of vehicle dynamics, e.g. acceleration time, which requires the inclusion of EM inertia (90)÷(91) presented in Section 4.3.

4.2. Electric motor efficiency characteristic

An EM is characterised by high efficiency in the whole work area, with the maximum value exceeding 97%. This section allows a formula for motor efficiency (75), as a function of its speed n and torque M, to be determined. The presented formula is based on 13 specific points (Fig. 7), that should come from measurements performed on a test rig.

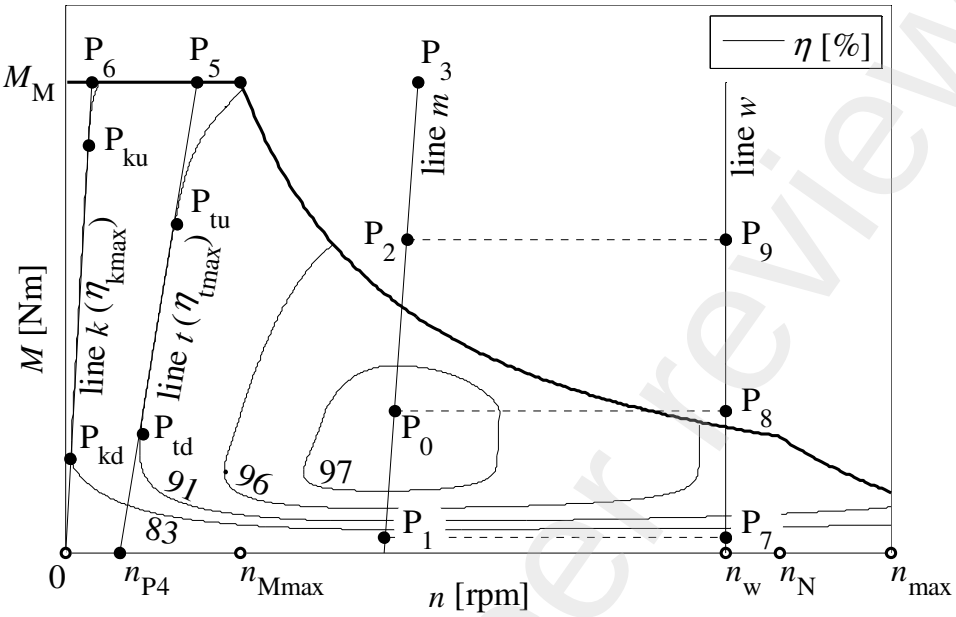

Fig. 7. EM efficiency characteristic.

Each point $P_0 \div P_9$ is determined by 3 values: n, M and η (except P_4 which requires only speed: n_{P4}). The specific conditions that allow the use of (75) are: $n_{P7}=n_{P8}=n_{P9}=n_w$, $M_{P7}=M_{P1}$, $M_{P8}=M_{P0}$, $M_{P9}=M_{P2}$, $M_{P1}<0.5M_{P0}$, $M_{P3}=M_{P5}=M_{P6}=M_M$, points: P_{kd}, P_{ku}, P_{td} and P_{tu} are determined only by M and line k always starts at (0, 0). The formula that allows the EM efficiency η_{EM} to be calculated is:

$$\eta_{EM}=\left\{\left[\frac{a_{II}-a_I}{1+0.01\text{^}(n-n_m)}+a_I\right]\cdot|n-n_m|\text{^}\left[\frac{2-p_I}{1+0.01\text{^}(n-n_m)}+p_I\right]+\eta_m\right\}\cdot\left[\frac{2}{1+0.01\text{^}(n/n_k)}-1\right] \quad (75)$$

where the variables depending on M are:

$$n_k=\frac{n_{P6}}{M_{P6}}\cdot M \quad (76)$$

$$n_t=\frac{n_{P5}-n_{P4}}{M_{P5}}\cdot M+n_{P4} \quad (77)$$

$$n_m=\frac{n_{P0}-n_{P1}}{M_{P0}}\cdot M+n_{P1} \quad (78)$$

$$\eta_k=\eta_{kmax}\cdot\left[\frac{2}{1+0.01\text{^}(M/M_{kd})}-1\right]\cdot\left[\frac{2\cdot(\eta_{P6}/\eta_{k\,max}-1)}{1+0.01\text{^}[(M-M_M)/(M_M-M_{ku})]}+1\right] \quad (79)$$

$$\eta_t=\eta_{tmax}\cdot\left[\frac{2}{1+0.01\text{^}(M/M_{td})}-1\right]\cdot\left[\frac{2\cdot(\eta_{P5}/\eta_{t\,max}-1)}{1+0.01\text{^}[(M-M_M)/(M_M-M_{tu})]}+1\right] \quad (80)$$

$$\eta_m=\left[\frac{a_{22}-a_{11}}{1+0.01\text{^}(M-M_{P0})}+a_{11}\right]\cdot|M-M_{P0}|\text{^}\left[\frac{pw_{22}-pw_{11}}{1+0.01\text{^}(M-M_{P0})}+pw_{11}\right]+\eta_{P0} \quad (81)$$

$$\eta_w=\eta_m\frac{\eta_{P8}}{\eta_{P0}}\cdot\left[1+\left(\frac{\eta_{P0}\eta_{P7}}{\eta_{P1}\eta_{P8}}-1\right)\cdot\left(\frac{-5}{M_{P7}^2}+1\right)\text{^}(M-M_{P7})^2\right]\cdot\left\{\frac{2\cdot[(\eta_{P0}\eta_{P9})/(\eta_{P2}\eta_{P8})-1]}{1+0.01\text{^}[(M-M_{P9})/(M_{P9}-M_{P8})]}+1\right\} \quad (82)$$

$$p_{\mathrm{I}} = \frac{\ln[(\eta_{\mathrm{t}} - \eta_{\mathrm{m}})/(\eta_{\mathrm{k}} - \eta_{\mathrm{m}})]}{\ln[(n_{\mathrm{t}} - n_{\mathrm{m}})/(n_{\mathrm{k}} - n_{\mathrm{m}})]} \tag{83}$$

$$a_{\mathrm{I}} = \frac{\eta_{\mathrm{k}} - \eta_{\mathrm{m}}}{|n_{\mathrm{k}} - n_{\mathrm{m}}| \wedge p_{\mathrm{I}}} \tag{84}$$

$$a_{\mathrm{II}} = \frac{\eta_{\mathrm{w}} - \eta_{\mathrm{m}}}{(n_{\mathrm{w}} - n_{\mathrm{m}})^2} \tag{85}$$

and the constant values:

$$pw_{11} = \frac{\ln[\eta_{\mathrm{P0}}/(\eta_{\mathrm{P0}} - \eta_{\mathrm{P1}})]}{\ln[M_{\mathrm{P0}}/(M_{\mathrm{P0}} - M_{\mathrm{P1}})]} \tag{86}$$

$$a_{11} = \frac{\eta_{\mathrm{P1}} - \eta_{\mathrm{P0}}}{(M_{\mathrm{P0}} - M_{\mathrm{P1}}) \wedge pw_{11}} \tag{87}$$

$$pw_{22} = \frac{\ln[(\eta_{\mathrm{P3}} - \eta_{\mathrm{P0}})/(\eta_{\mathrm{P2}} - \eta_{\mathrm{P0}})]}{\ln[(M_{\mathrm{P3}} - M_{\mathrm{P0}})/(M_{\mathrm{P2}} - M_{\mathrm{P0}})]} \tag{88}$$

$$a_{22} = \frac{\eta_{\mathrm{P2}} - \eta_{\mathrm{P0}}}{(M_{\mathrm{P2}} - M_{\mathrm{P0}}) \wedge pw_{22}} \tag{89}$$

The above formulas allow the efficiency in static states to be determined. In dynamic states, the inertia must be taken into account, which is described in Section 4.3.

4.3. Dynamic states

In dynamic states (e.g. at ICE start), the EM rotor inertia J_{EM} generates additional resistance torque, which influences the dynamic torque M_{dyn}:

$$M_{\mathrm{dyn}} = M - J_{\mathrm{EM}} \cdot \varepsilon_{\mathrm{EM}} \tag{90}$$

where the EM inertia J_{EM} can be estimated as:

$$J_{\mathrm{EM}} = 0.001 \cdot (0.125 \cdot M_{\mathrm{M}} + 3.75) \tag{91}$$

The EM operates with high angular acceleration exceeding 1000 rad/s^2, which may consume over 20% of the total EM torque.

4.4. EM start

The start process refers to an EM which propels the ICE. Sometimes it is called a generator (GEN). The start torque is needed to put the EM into motion when it starts the ICE. The power from the BAT propels not only the ICE but also overcomes EM inertia. The torque generated by EM inertia during the ICE start is:

$$M_{\mathrm{EM\_start}} = J_{\mathrm{EM}} \cdot \varepsilon_{\mathrm{EM}} \tag{92}$$

The additional power $N_{\mathrm{EM\_start}}$ for the ICE start is:

$$N_{\mathrm{EM\_start}} = \frac{M_{\mathrm{EM\_start}} \cdot n_{\mathrm{EM\_start}}}{9550} \tag{93}$$

The $n_{\mathrm{EM\_start}}$ is the speed when the largest power is needed (67) during the ICE start.

5. Inverter characteristic

The inverter (INV) changes the parameters of electric power (voltage and current) and converts direct current from the BAT to alternating current propelling the EM, or vice versa. The INV efficiency η_{INV} depends on the power transferred N^{rel} (Fig. 8). The formula that allows the η_{INV} to be calculated is:

$$\eta_{\mathrm{INV}}(N^{\mathrm{rel}}) = -a_0 \cdot \left| N^{\mathrm{rel}} - N^{\mathrm{rel}}_{\mathrm{P0}} \right| \wedge p_0 + \eta_{\mathrm{P0}} \tag{94}$$

where N^{rel} is the ratio of the actual power transmitted by the INV to its nominal power (which is the nominal power of the relevant EM).

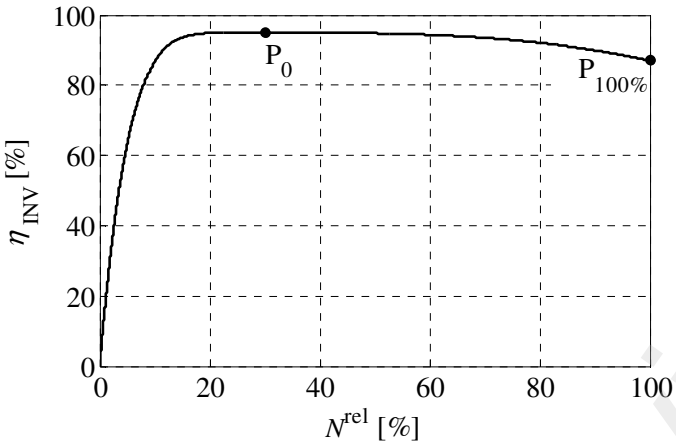

Fig. 8. Inverter efficiency vs transferred power.

The variables are the following:

$$p_0 = \frac{-p}{1+0.01\text{^}(N^{\text{rel}} - N_{\text{P0}}^{\text{rel}})} + 2 \cdot p \tag{95}$$

$$a_0 = \frac{(\eta_{\text{P0}} - \eta_{\text{P100}}) / (100 - N_{\text{P0}}^{\text{rel}})\text{^}\, p_0 - \eta_{\text{P0}} / (N_{\text{P0}}^{\text{rel}})\text{^}\, p_0}{1+0.01\text{^}(N^{\text{rel}} - N_{\text{P0}}^{\text{rel}})} + \frac{\eta_{\text{P0}}}{(N_{\text{P0}}^{\text{rel}})\text{^}\, p_0} \tag{96}$$

where p=2÷3.

6. Battery in a hybrid drivetrain

6.1. Battery – general overview

A BAT in a hybrid drivetrain has multiple tasks: it realizes the ICE stop-start function, enables the vehicle to move in an EV mode, recuperates kinetic energy or supports the ICE. Total capacity (*CAP*) in a full-hybrid vehicle is *CAP*=(0.9÷2.2) kWh, whereas in a mild-hybrid *CAP*=(0.2÷0.8) kWh with regard to m_t and V_{ICE}.

A BAT consists of n_{cell} cells usually connected in series. Most commonly, high performance lithium-ion or lithium-polymer cells, with the nominal voltage of U_{nom}=3.7 V, are used. These cells are characterized by a very low internal resistance (R<5 mΩ at 25°C) [27] allowing a high discharge and charge current to be transferred with high efficiency. A single cell is characterized by a rated capacity *RC* [Ah] (usually *RC*=4÷6 Ah) and *C*-rate (C_{rate}) [1/h] expressing discharge intensity. The current *I* [A] of a single cell is $I=C_{\text{rate}} \cdot RC$.

Lithium-ion cells are characterized by gravimetric energy density ρ_{G}≈80 Wh/kg [63], volumetric energy density ρ_{V}≈150 Wh/dm^3 [63], massic density ρ≈1.9 kg/dm^3 and specific heat C_{sh}≈900÷1000 J/kgK [64, 65]. Cell temperature is constantly measured because it influences the BAT performance significantly and should not exceed 35°C [66] to achieve vehicle lifetime durability.

To perform in the area of the lowest internal resistance *R* level (high efficiency and low temperature gradients) and provide the longest possible life of a lithium-ion battery, they operate within 30÷80% state of charge (*SOC*), so on average only half of *CAP* is available to propel the vehicle in the EV mode. In fact, the useful range is even smaller, because the BAT must always be ready for an e-boost and recharging. This means that the degree of discharge ψ (ψ=1-*SOC*) usually varies by 25%*CAP*. The peak *C*-rate for automotive applications is currently $C_{\text{rate\_peak}}$≈40. *C*-rate is connected with the time the BAT supplies the power (or is charged). The higher the *C*-rate the shorter the time. To provide a lifetime durability of the BAT and good performance, the following *C* ratings for lithium-ion BATs should be followed: for a short time maximum-power operation (hard braking or vehicle propulsion plus ICE start) $C_{\text{rate\_max}} \approx (0.8 \div 0.9) \cdot C_{\text{rate\_peak}}$, for an intermittent operation lasting about 10÷20 s:

$C_{rate\_int} \approx (0.5 \div 0.6) \cdot C_{rate\_max}$ (dynamic acceleration or deceleration), and for continuous work [67] $C_{rate\_cont} < (0.10 \div 0.15) \cdot C_{rate\_max}$ (ICE support or BAT charging in generally steady conditions). With the comfortable cabin temperature t_{cab}=25°C [68], the above BAT working states may occur repeatedly, one after another and it will not lead to a BAT temperature increase above 35°C (example in Section 6.4).

6.2. Single cell voltage vs degree of discharge characteristics

For a detailed analysis of the charge and discharge process, the voltage U of a single lithium-ion cell vs degree of discharge (ψ) characteristic, presented in Fig. 9, can be used. The upper solid line represents the characteristic U_0 when no current draws through the cell. The bottom dotted line represents cell voltage when it provides the maximum current I_{max}.

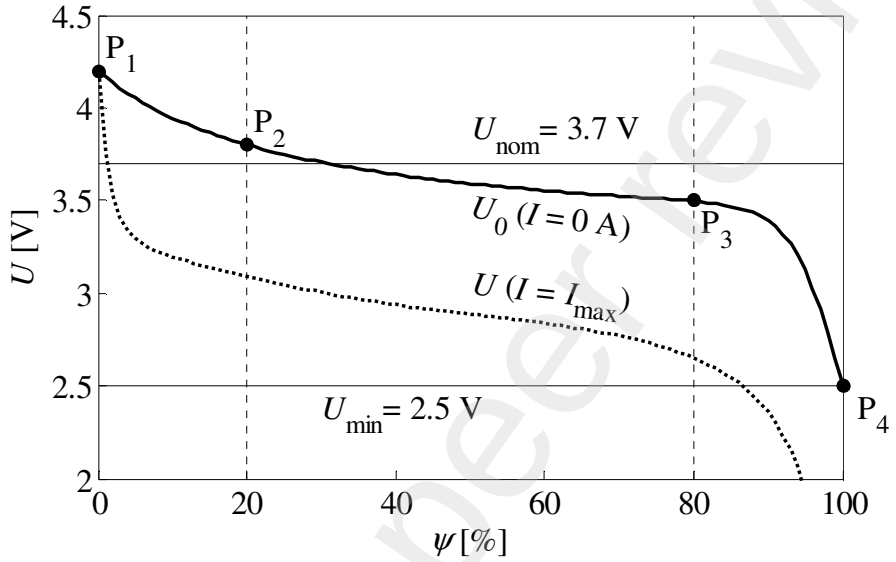

Fig. 9. Voltage U vs degree of discharge ψ.

The voltage U_0 of the battery versus ψ can be described by the following formula:

$$U_0(\psi) = U_{P1} - \left(\frac{\psi}{a_1 + \psi} \right) \cdot k_1 \tag{97}$$

where the constants are:

$$a_1 = \frac{\psi_{P2} \cdot \psi_{P3} \cdot (U_{P2} - U_{P3})}{\psi_{P2} \cdot (U_{P3} - U_{P1}) - \psi_{P3} \cdot (U_{P2} - U_{P1})} \tag{98}$$

$$k_1 = \frac{2 \cdot [(U_{P2} - U_{P1}) \cdot (1 + a_1 / \psi_{P2}) + (U_{P1} - U_{P4}) \cdot (1 + a_1 / 100)]}{1 + \exp\{[-6 \cdot (\psi - \psi_{P4}) / (100 - \psi_{P3})]\}} + (U_{P1} - U_{P2}) \cdot (1 + a_1 / \psi_{P2}) \tag{99}$$

To draw the characteristic of U_0, four points must be determined: P_1, P_2, P_3 and P_4. To obtain a full voltage characteristic, for different currents and temperatures, the internal resistance R [Ω] must also be known. Fig. 10 presents R vs ψ for a lithium-ion cell at different working temperatures [26, 27, 28, 69]. There is an additional point P_0 with corresponding R_{P0} (minimum value of resistance). The internal resistance R^{25} of a single cell at 25°C is:

$$R^{25}(\psi) = \left[\frac{R_{P4} - R_{P1}}{1 + 0.01\text{^}(\psi - \psi_{P0})} + R_{P1} - R_{P0} \right] \cdot \left| \frac{\psi - \psi_{P0}}{\frac{100 - 2 \cdot \psi_{P0}}{1 + 0.01\text{^}(\psi - \psi_{P0})} + \psi_{P0}} \right| \text{^} \left[\frac{p_2 - p_1}{1 + 0.01\text{^}(\psi - \psi_{P0})} + p_1 \right] + R_{P0} \tag{100}$$

where:

$$p_1 = \log[(R_{P2} - R_{P0}) / (R_{P1} - R_{P0})] / \log[(\psi_{P0} - \psi_{P2}) / \psi_{P0}] \tag{101}$$

$$p_2 = \log[(R_{P3} - R_{P0}) / (R_{P4} - R_{P0})] / \log[(\psi_{P3} - \psi_{P0}) / (100 - \psi_{P0})] \tag{102}$$

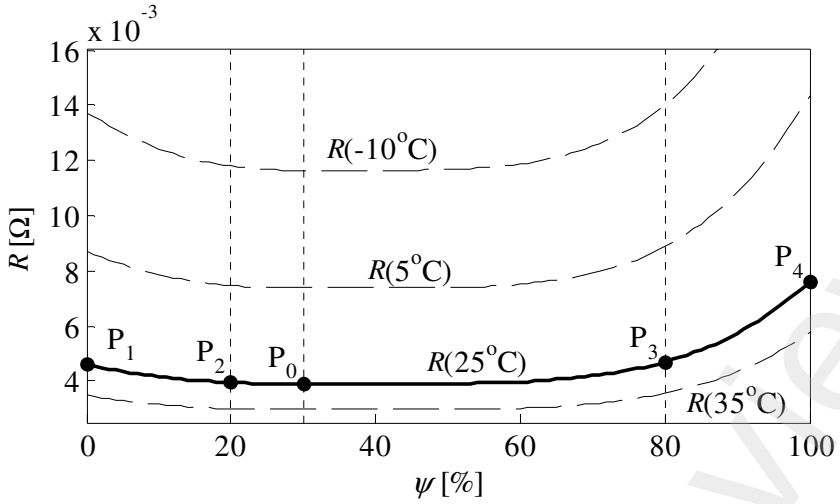

Fig. 10. Resistance vs degree of discharge for a lithium-ion cell.

At low temperatures, cell performance deteriorates due to increased resistance. The coefficient C_R (varies from C_R=3 for -10°C to C_R=0.5 at 50°C) represents the change of cell R in relation to its temperature:

$$C_R = 2.2 \cdot 0.969\text{^}temp_{cell} \tag{103}$$

Finally, the formula for R, in the temperature range of -10÷30°C, is:

$$R = R^{25} \cdot C_R \tag{104}$$

When the actual value of cell resistance R is already calculated, one can use basic relationships to calculate its performance. Cell power is:

$$N_{cell} = 0.001 \cdot I \cdot \left[U_0(\psi) - R \cdot I\right] \tag{105}$$

and cell efficiency (subscripts for discharging, superscripts for charging):

$$\eta_{cell} = \left(\frac{U_0}{U_0 \pm I \cdot R} \right)^{\pm 1} \tag{106}$$

Lithium-ion cells have a minimum voltage of 2.5 V.

6.3. Battery total capacity

CAP in a full-hybrid vehicle is important, because it influences parameters in the EV mode: vehicle acceleration, speed and range. Moreover, the larger the *CAP* the smaller its temperature increase, which is desired. However, the BAT cannot be too large, so as not to increase vehicle weight and its cost. The nominal voltage usually exceeds 180 V and in the case of series design is the sum of each cell voltage. The parameters of a single cell are: U_{nom}, RC, C_{rate_peak} and R. The BAT parameters are:

$$U_{BAT} = n_{cell} \cdot U_{nom} \tag{107}$$

$$CAP = 0.001 \cdot U_{BAT} \cdot RC \tag{108}$$

$$N_{BAT} = N_{cell} \cdot n_{cell} \tag{109}$$

A properly-sized BAT allows gentle city driving in the EV mode without the assistance of the ICE. This can be assessed based on the WLTP vehicle speed profile, where moderate acceleration in average city traffic is 0.8÷1.1 m/s^2 to the speed of 40÷50 km/h (the product of $a_v \cdot v$<30). The required BAT power N_{BAT} which allows vehicle propulsion (for C_{rate_int}) is:

$$N_{BAT\_Cint} = \frac{m_t \cdot \delta \cdot a_v \cdot (v/3.6)}{1000 \cdot \eta_{tr} \cdot \eta_{INV}} \approx 0.01 \cdot m_t \tag{110}$$

Then n_{cell} (109) and *CAP* (108) are calculated. The power N_{BAT_Cint} (110) refers to intermittent operation. It increases BAT durability and leaves the reserve of C_{rate}≈10, allowing an additional short-time power (C_{rate_max}) to start the ICE (67):

$$N_{\mathrm{BAT\_Cmax}} = N_{\mathrm{BAT\_Cint}} + \left(\frac{N_{\mathrm{ICE\_start}}}{\eta_{\mathrm{EM\_ICE}}} + \frac{N_{\mathrm{EM\_start}}}{\eta_{\mathrm{EM}}} \right) \cdot \frac{1}{\eta_{\mathrm{INV}}} \tag{111}$$

The calculated *CAP* is capable of full recuperation of kinetic energy under normal braking.

The maximum speed in the EV mode v_{maxEV} can be calculated with the use of (129). The maximum range in the EV mode s_{EV} [m] to be travelled at constant speed should also be verified. When a traction EM works at low load, its INV efficiency is low and varies within a wide range η_{INV}≈20÷80% influencing the range s_{EV} significantly:

$$s_{\mathrm{EV}} = \frac{3.6 \cdot 10^6 \cdot (25\% \cdot CAP) \cdot \eta_{\mathrm{tr}} \cdot \eta_{\mathrm{INV}} \cdot \eta_{\mathrm{BAT}}}{F_{\mathrm{roll}} + F_{\mathrm{aero}}} \tag{112}$$

A mild-hybrid drivetrain is equipped with a relatively small BAT with a nominal voltage of 48 V, which has the main task of providing electrical power that allows a quick ICE start, recuperate kinetic energy and support the ICE during acceleration. The power N_{BAT} (for $C_{\mathrm{rate\_max}}$) delivered to the crankshaft at the ICE start is:

$$N_{\mathrm{BAT\_Cmax}} = \left(\frac{N_{\mathrm{ICE\_start}}}{\eta_{\mathrm{vb}}} + \frac{N_{\mathrm{EM\_start}}}{\eta_{\mathrm{EM}}} \right) \cdot \frac{1}{\eta_{\mathrm{INV}}} \tag{113}$$

Because in the mild-hybrid transmission *CAP* is relatively small, the use of an additional conventional 12 V battery for cold ICE starts should be considered.

6.4. Thermal behaviour of the BAT

An example of thermal behaviour (Fig. 11) is based on a B-class vehicle with a series full-hybrid drivetrain and the following parameters: m_{t}=1350 kg, $C_{\mathrm{d}}A$=0.6 m^2, R_{d}=0.3 m and V_{ICE}=1.5 dm^3. The BAT with *CAP*=0.9 kWh consists of 60 prismatic lithium-ion cells (4 Ah and 3.7 V each) connected in series, with the dimensions 12 x 70 x 110 [mm], resulting in A_{cell}≈0.02 m^2, V_{cell}≈0.09 dm^3, R^{25}=4 mΩ and m_{cell}≈0.2 kg.

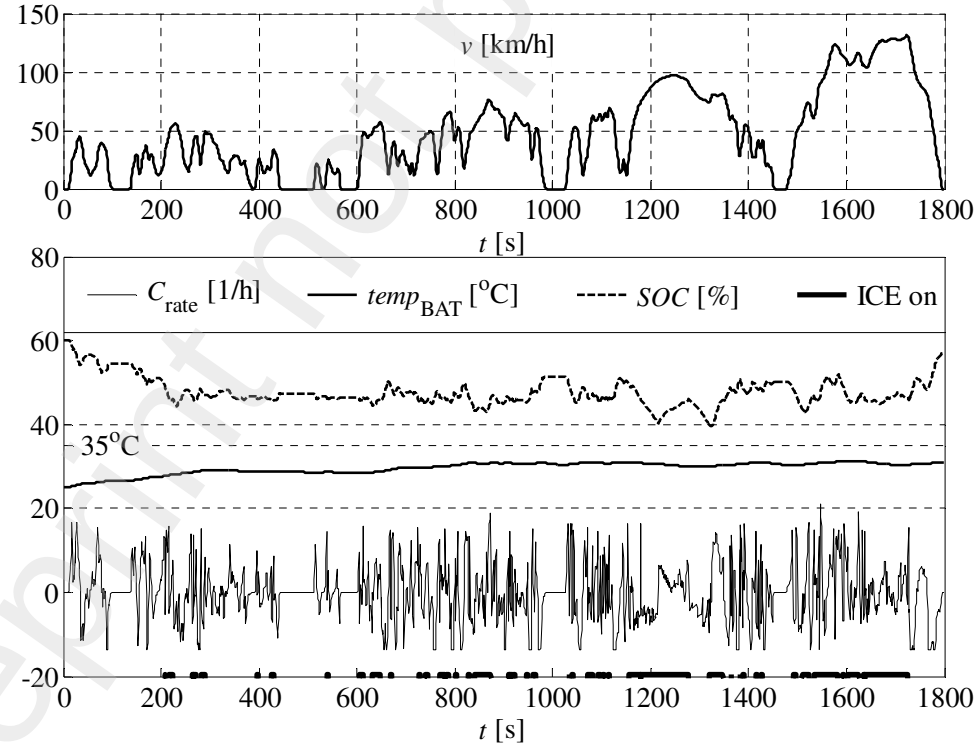

Fig. 11. Thermal behaviour of a BAT in the WLTP cycle.

The simplified model of uniform thermal behaviour of a cell is:

$$\Delta temp_{\mathrm{cell}} = [0.001 \cdot N_{\mathrm{cell}} \cdot (1 - \eta_{\mathrm{cell}}) - h_{\mathrm{air}} \cdot A_{\mathrm{cell}} \cdot (t_{\mathrm{cell}} - t_{\mathrm{cab}})] \cdot \Delta t / (C_{\mathrm{sh}} \cdot m_{\mathrm{cell}}) \tag{114}$$

where h_{air}=(5÷30) W/m^{2}K (smallest value for BAT fan off, largest for fan max speed).

7. Transmission efficiency

Total transmission efficiency depends on the efficiency of each component: gears, clutches, shafts, roller bearings, etc. Maximum efficiency of each element [70], occurs at 60÷100% of nominal power transferred (Fig. 12).

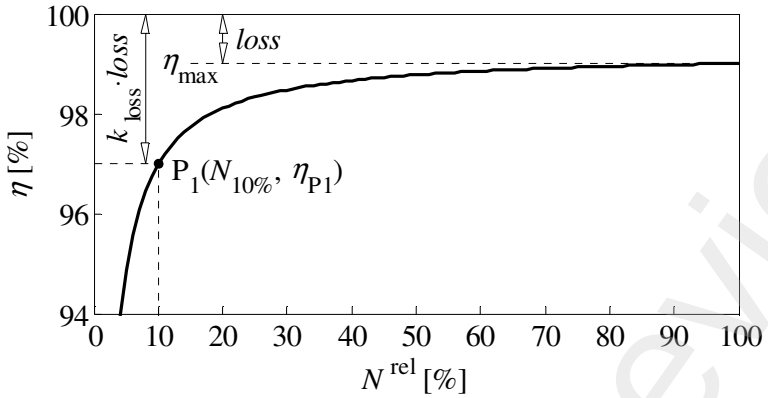

Fig. 12. Component efficiency vs transferred power.

In reality, the efficiency of e.g. gearwheels, bearings and multirib v-belt is not constant and varies with regard to the transferred load. Measurements [71] indicate the relationship presented in Fig. 12. The coefficient $k_{\text{loss}}=(3\div4)\cdot loss$ for most applications. The formula for the efficiency is:

$$\eta[\%]=\left[\frac{N^{\text{rel}}}{N^{\text{rel}}+\dfrac{100\cdot(\eta_{\max}-\eta_{\text{P1}})}{10\cdot\eta_{\text{P1}}-\eta_{\max}}}\right]\cdot\frac{9\cdot\eta_{\text{P1}}\cdot\eta_{\max}}{10\cdot\eta_{\text{P1}}-\eta_{\max}} \tag{115}$$

In the initial drivetrain calculations the following values can be used: $\eta_{\text{tr}}\approx90\%$ for MT (mechanical transmission), AMT (automated mechanical transmission) and dry DCT, $\eta_{\text{tr}}\approx87\%$ for wet DCT, $\eta_{\text{tr}}\approx83\%$ for AT (automatic transmission with planetary gear sets) and e-CVT (series hybrids).

8. Inertia of rotating elements

Rotational elements in vehicles generate inertia, which must be taken into account during the vehicle design process. As mentioned in Section 2, the coefficient δ refers only to the inertia of wheels (tyres J_{tyre} and rims J_{rim}) and brakes J_{brk}:

$$\delta=1+\frac{\Sigma\left(J_{\text{rim}}+J_{\text{tyre}}+J_{\text{brk}}\right)}{m_{\text{t}}\cdot R_{\text{d}}^2} \tag{116}$$

Formulas 117÷118 [72] present the moments of inertia of rims J_{rim} and tyres J_{tyre}:

$$J_{\text{rim}}=[0.0075\cdot\left(D_{\text{rim}}-12\right)^2+0.065]\cdot k_{\text{rim}} \tag{117}$$

$$J_{\text{tyre}}=0.009\cdot\left(D_{\text{rim}}-9\right)^2+k_{\text{tyre}} \tag{118}$$

where D_{rim} is a rim diameter in [inch], $k_{\text{tyre}}=0.00$ for a summer tyre and $k_{\text{tyre}}=0.12$ for a winter tyre. Fig. 13 presents three designs of alloy rims which influence their inertia. Steel rim design is quite common, thus the moment of inertia for this one depends only on its size.

Formula 119 presents moments of inertia of standard disc brakes (front are ventilated $k_{\text{brk}}=2.7$ and rear are solid $k_{\text{brk}}=1.0$):

$$J_{\text{brk}}=(2.6\cdot10^{-6}\cdot N_{\text{N\_ICE}}^2+0.009)\cdot k_{\text{brk}} \tag{119}$$

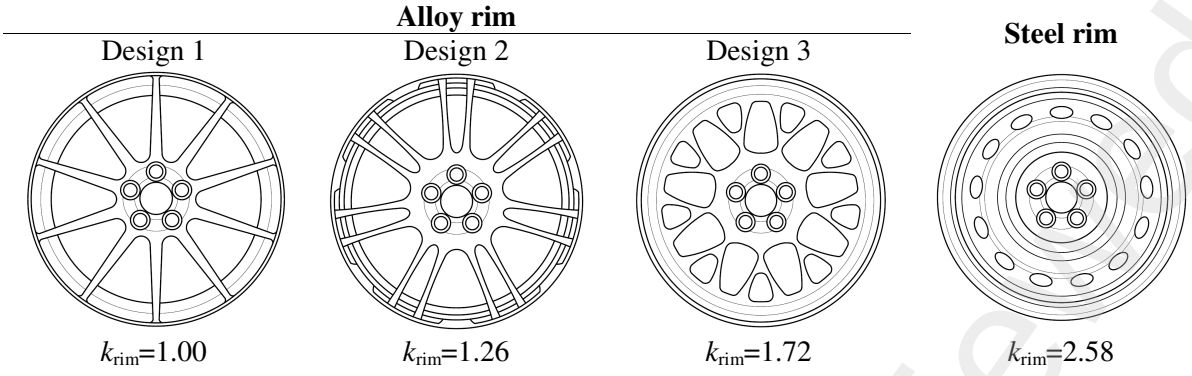

Fig. 13. Shapes of rims.

In the transmission, there might be also a gearbox which the moment of inertia J_{gbx} can be reduced to the axis of the wheels, similarly to disc brakes [73]. However, architectures of hybrid transmissions (Sections 10.2÷10.5) vary significantly, so this factor must be determined individually.

9. Basic drivetrain calculations

9.1. Maximum gear ratio

The first factor concerns moving off on a slope (Fig. 1). It determines the first gear total ratio i_{t1} in a mild-hybrid and parallel full-hybrid or just the reduction ratio in series and series-parallel hybrids for an EM. Every car must be capable of moving off on a slope of 26%. Formula (120) allowing a first gear ratio to be calculated concerns: FWD cars (which are most prone to tyre slipping), μ=0.8, h_c=0.5 m, l_b=l_f=1.35 m, a_h=0.8 m/s^2 and f_{roll}=0.015. Taking the above mentioned values and (1)÷(8), the total transmission in the first gear is:

$$i_{t1} > 3.4 \cdot \frac{m_{gross} \cdot R_d}{\eta_{tr} \cdot M(2500)} \tag{120}$$

In the denominator, there is $M(2500)$ instead of M_M, because in the case of an ICE, which develops M_M at n_{M1}>2500 rpm, the clutch is extremely exposed to overheating.

The second factor concerns moving off on a flat road with the maximum acceleration $a_{\mu max}$ from a standstill on the grip limit. For a vehicle with parameters like in the previous section, and mass m_t=1.2·m_e, the maximum acceleration is: $a_{\mu max}$≈3.4 m/s^2 for FWD, $a_{\mu max}$≈4.6 m/s^2 for RWD, and $a_{\mu max}$≈7.9 m/s^2 for AWD vehicles. Based on (1)÷(8), the minimum ratio in first gear that allows a grip limit to be fully utilized can be calculated based on:

$$i_{t1} > \frac{m_t \cdot (a_{\mu max} \cdot \delta + g \cdot f_{roll}) \cdot R_d}{M_{M\_ICE/EM} \cdot \eta_{tr}} \tag{121}$$

The third factor takes into consideration dry friction clutch durability in a mild-hybrid MT or AMT transmission. The i_{t1} ratio should be relatively high to ensure nominal clutch durability of 250 000 km. For this condition, the following assumptions are made [74, 75, 76]: a standard clutch material with friction coefficient μ_{cl}=0.4, specific wear 9 mm^3/MJ, maximum wear per side of clutch lining of g_{cl}=1 mm, permissible pressure p_{nom}=0.2 MPa on a clutch lining, safety coefficient of a clutch β=1.7 and δ_{cl}=0.65 (the ratio of inside to outside clutch lining diameter). The outer diameter of the clutch D_{cl} [mm] is:

$$D_{cl} = 28.8 \cdot \sqrt[3]{\frac{\beta \cdot M_M}{1 - \delta_{cl}^3}} \tag{122}$$

The clutch lining one side area A_{cl} [mm^2] is:

$$A_{cl} = \frac{\pi}{4} \cdot D_{cl}^2 \cdot \left(1 - \delta_{cl}^2\right) \tag{123}$$

The total volume of clutch linings V_{cl} [mm^3] is:

$$V_{cl} = 2 \cdot g_{cl} \cdot A_{cl} \tag{124}$$

Driving conditions are the following [70, 77]: 50% of city driving with 3 starts/1 km, 50% extra-urban driving with 0.2 starts/1 km including 2% of uphill starts (α=15%), average vehicle load is half of the maximum load (m_t=1.2·m_e) and the ICE speed while moving off on a flat road: n_{st} ≈1500 rpm, and n_{st} ≈2500 rpm on a hill to avoid ICE stalling and to develop sufficient torque. The minimum first gear ratio is:

$$i_{t1} > 0.17 \cdot R_d \cdot n_{st} \cdot \sqrt{m_t / V_{cl}} \tag{125}$$

In the case of a mild-hybrid DCT drivetrain, where the odd gear clutch transfers torque also during gear-changes: β=2.3, δ_{cl}=0.60 and g_{cl}=1.5 mm.

In the case of a full-hybrid DCT drivetrain most starts from a standstill are realized by an EM, which results in: β=1.8, δ_{cl}=0.65 and g_{cl}=1.5 mm.

The fourth factor concerns clutch warm-up while moving off on a slope of 15%, with the average acceleration a_{hst}=1.0 m/s^2 and n_{st}<2500 rpm, where the unit friction work should not exceed 2.2 J/mm^2 [74] (under these conditions, the average temperature of the clutch assembly rises ~25^{o}C in a single start). Based on (1)÷(8) and (123), this results in:

$$i_{t1} > 151 \cdot R_d \cdot \sqrt{m_{gross} / A_{cl}} \tag{126}$$

To avoid vehicle jerking [78÷80], the i_{t1} (selected from the above conditions) should not be additionally increased. Then the v_{N1} can be calculated:

$$v_{N1} = \frac{R_d \cdot n_N}{2.653 \cdot i_{t1}} \tag{127}$$

which will be used further in Section 10.2 in intermediate gear ratio calculations.

9.2. Maximum speed gear ratio

The maximum speed v_{max} of a vehicle is a constant speed that can be developed on a flat, dry road, without wind, with the throttle fully opened. In the case of a hybrid vehicle, v_{max} is calculated for the maximum power of the ICE only.

The aspect of maximum speed calculation can be considered in two ways. In the first one, v_{max} is assumed and N_w (power on the driven wheels) is calculated:

$$\left[0.5 \cdot \rho_{air} \cdot C_d \cdot A \cdot \left(\frac{v_{max}}{3.6}\right)^2 + m_t \cdot g \cdot f_{roll}\left(v_{max}, p_{tyre}, G_t\right)\right] \cdot \frac{v_{max}}{3600} = N_w \tag{128}$$

In the second attempt, N_w is assumed and v_{max} is searched. To avoid numerical computations, one can use the following formula:

$$v_{max} = 48 \cdot \sqrt[3]{N_w} - 70 \cdot \sqrt{C_d A} - 1.5 \cdot \sqrt{m_t} + 3 \cdot p_{tyre} - 6 \cdot \alpha_{\%} + 94.4 \tag{129}$$

For both (128) and (129): N_w=N_{ICE}(n_{vmax})·k_{chg}·η_{tr}. The maximum speed v_{max} is reached at n_{vmax}=(0.90÷1.05)·n_N (according to Table 4). The coefficient k_{chg}=(0.95÷0.98) takes into account the need for BAT recharging, after depletion during acceleration to v_{max}. The tyre pressure p_{tyre} may vary only within the range accepted by the manufacturer and road slope varies 0÷6%. This formula can also be used for calculations of v_{maxEV} (Section 6.3). The above calculations allow a maximum speed ratio to be calculated:

$$i_{tv\,max} = \frac{R_d \cdot n_{vmax}}{2.653 \cdot v_{max}} \tag{130}$$

10. Matching hybrid transmission

10.1. Assumptions and initial calculations

Input parameters for calculations are: A, C_d, R_d, m_e and desired v_{max}. They allow N_N of the ICE to be calculated. Then, based on (9)÷(10) and Table 1: n_N, M_M, n_M and V_{ICE} are determined. The BAT size (*CAP*) is calculated with the use of (107)÷(110).

Sections 10.2÷10.5 describe further steps for each type of transmission which concerns calculations of the EM and GEN torque and power as well as gear ratios in a transmission.

10.2. Mild-hybrid transmission

In a mild-hybrid drivetrain (Fig. 14), a low-power EM (called a belt starter generator - BSG), propelled by a multirib v-belt, is used.

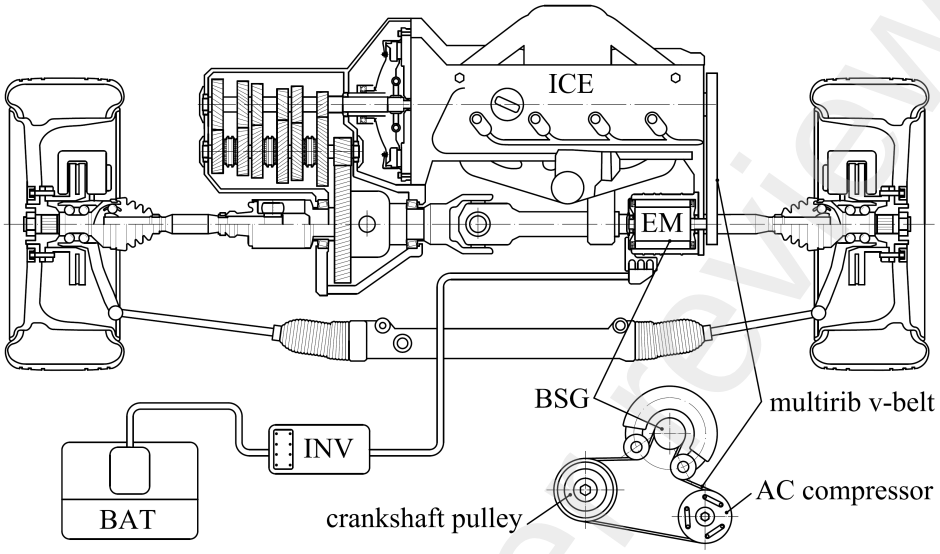

Fig. 14. Mild-hybrid 6-speed manual transmission.

Such propulsion is frequently based on a stepped manual or automatic gearbox. The first gear ratio i_{t1} is calculated with regard to (120)÷(126). Then the gear number for v_{max} (128) is set based on Table 4.

Table 4

Vehicle maximum speed gear and corresponding ICE speed selection.

N_N [kW]:	50	60	70	90	100	140
z:	5		6		7 / 8	
eco	0.85	0.85	0.85	0.90	0.85	0.90
↑	k_v	k_v	k_v	k_v	k_v	k_v
↓	1.10	1.00	1.05	1.00	1.00	0.95
dyn						

(k) - gear for maximum speed, z - total number of forward gears, $k_v = n_{vmax} / n_N$

Then, intermediate gears in stepped transmissions: MT, AT, AMT and DCT, are calculated (Fig. 15), similarly to [71].

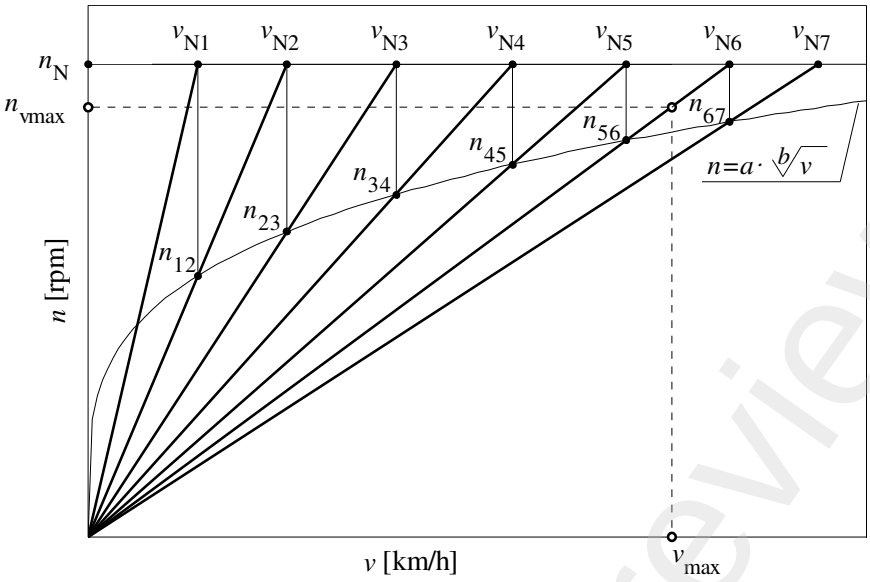

Fig. 15. Method of calculating intermediate gears in a stepped transmission.

The presented model assumes an upshift at n_N in the x^{th} gear. It starts with x=1:

$$v_{Nx} = \frac{R_d \cdot n_N}{2.653 \cdot i_{tx}} \tag{131}$$

Then, the ICE speed n_{xy} after an upshift from the x^{th} gear to the y^{th} gear (y=x+1), at the nominal engine speed n_N, is calculated based on the following formula:

$$n_{xy} = a \cdot \sqrt[b]{v_{Nx}} \tag{132}$$

Next, the gear ratio of the following gear is calculated:

$$i_{ty} = \frac{R_d \cdot n_{xy}}{2.653 \cdot v_{Nx}} \tag{133}$$

Then, the next gear ratios are calculated in a similar way, one after another. The formula for the coefficient a is [70]:

$$a = \left\{ \frac{\frac{n_N}{n_{vmax}} \cdot v_{max}}{n_N \wedge \left[\frac{b^{k-1} - (b-1)^{k-1}}{b^{k-2}} \right] \cdot v_{N1} \wedge \left[\frac{(b-1)^{k-1}}{b^{k-1}} \right]} \right\} \wedge \left[\frac{b^{k-2}}{(b-1)^{k-1} - b^{k-1}} \right] \tag{134}$$

The coefficient b=3.0÷4.0. A smaller value narrows high gears (suggested for an NA ICE), while a higher value evenly distributes all gears (suggested for a TB ICE).

In a mild-hybrid transmission, the EM is permanently connected with the ICE by a multirib v-belt, which limits the power that can be transferred to 10÷15 kW. The belt ratio is i_{EM_ICE}=2.000÷2.500. The EM torque is calculated based on (65) and (92):

$$M_{M\_EM} = M_{EM\_start} + \frac{M_{ICE\_start}}{i_{EM\_ICE} \cdot \eta_{vb}} \tag{135}$$

The rated speed is:

$$n_{Mmax} = n_{ICE\_start} \cdot i_{EM\_ICE} \tag{136}$$

Then, the nominal power N_{N_EM} is calculated (68). In contrast with a conventional 12 V starter, the mild-hybrid allows a higher ICE speed of n_{ICE_start}≈1000 rpm to be reached before the combustion process starts in cylinders. This results in the smooth work of the ICE without vibrations and shuddering. A small lithium-ion battery has the *CAP* based on (113).

10.3. Parallel full-hybrid transmission

In a parallel full-hybrid transmission (Fig. 16), which is always equipped with an automatic transmission, a high-torque EM is mounted on the clutch cover.

The EM can assist the ICE, propel the vehicle itself in the EV mode or recuperate the kinetic energy of a vehicle. To ensure this, there is always a disconnecting clutch between the ICE and main clutch(es).

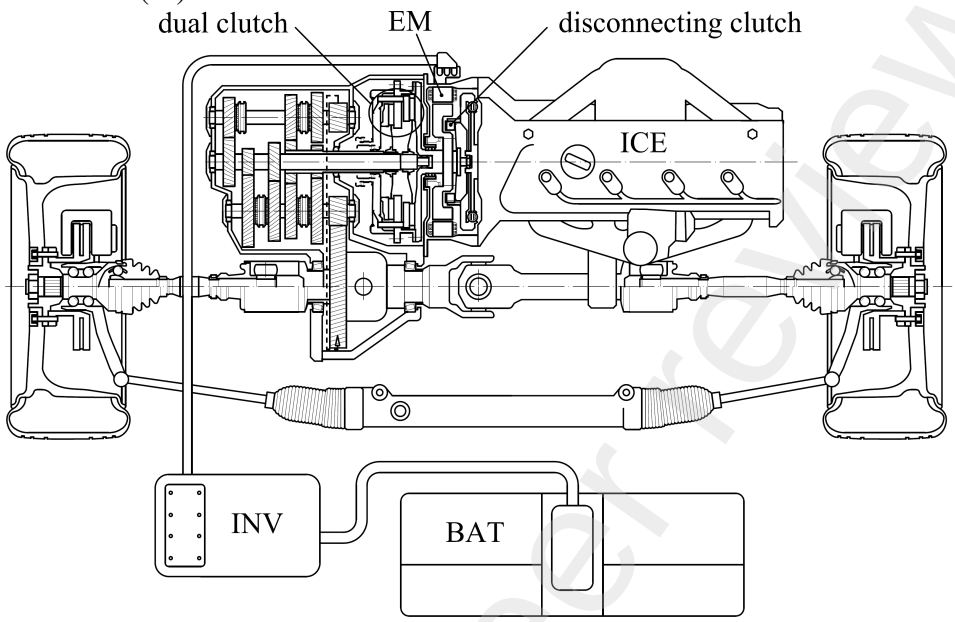

Fig. 16. Parallel hybrid transmission.

The first gear ratio in a parallel-hybrid transmission is calculated only for ICE torque, in the case the vehicle starts uphill with the BAT depleted. Its value is based on conditions (120)÷(126). The maximum speed ratio is calculated based on (130), and intermediate gears are calculated similarly to a mild-hybrid stepped transmission (131)÷(134).

In a full-hybrid transmission, the EM torque should allow moderate acceleration $a_v \approx 0.8 \div 1.1$ m/s^2 up to 40÷50 km/h, which can be realized in 2nd or 3rd gear.

Due to the lowest ratio in 3rd gear, this one is considered. Moreover, at this state, the EM must have enough torque reserve to start the ICE. Thus, the formula for the EM nominal torque is:

$$M_{\mathrm{M\_EM}} > \frac{\left[a_{\mathrm{v}} \cdot \delta \cdot m_{\mathrm{t}} + F_{\mathrm{roll}}(50\ \mathrm{km/h}) + F_{\mathrm{aero}}(50\ \mathrm{km/h})\right] \cdot R_{\mathrm{d}}}{i_{\mathrm{t3}} \cdot \eta_{\mathrm{tr}}} + M_{\mathrm{ICE\_start}} \tag{137}$$

and power (111):

$$N_{\mathrm{N\_EM}} = N_{\mathrm{BAT\_Cmax}} \cdot \eta_{\mathrm{INV}} \cdot \eta_{\mathrm{EM}} \tag{138}$$

The rated speed n_{Mmax} of the EM is calculated with (68). It is preferable to obtain $n_{\mathrm{Mmax}} \approx n_{\mathrm{M1}}$, which allows the ICE low torque to be filled by the EM.

10.4. Series full-hybrid drivetrain

A series hybrid drivetrain is presented in Fig. 17. In this case, the driven wheels are propelled only by an EM, which has to be rated for the maximum power requirement of the vehicle. This makes this drivetrain similar to a BEV. The difference is that a small BAT can power the EM only for a short time and with power limited by the BAT power. In the case of rapid acceleration or high speed driving, the electric power for the EM comes not only from the BAT but also from the GEN propelled by the ICE. The GEN must be properly matched with the ICE so that their areas with maximum efficiencies coincide.

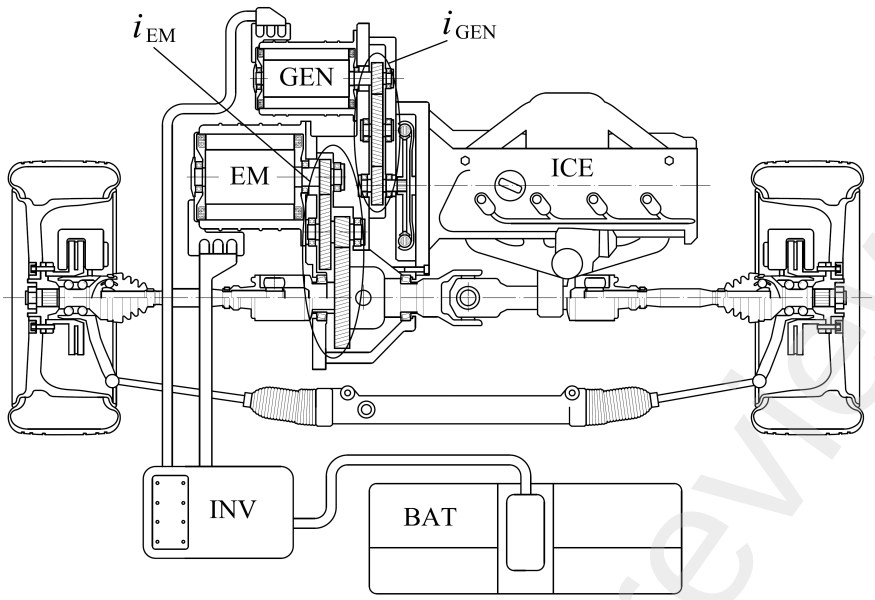

Fig. 17. Series hybrid drivetrain.

The ratio between the GEN and ICE equals:

$$i_{GEN\_ICE} = \frac{n_{N\_GEN}}{n_{N\_ICE}} \tag{139}$$

Fig. 18 presents the GEN characteristic matched to the ICE characteristic (e.g. i_{GEN_ICE}=1.333 in Fig. 18). Dashed lines represent the optimum operating curve. Nominal GEN power equals nominal ICE power decreased by the gear efficiency $\eta_{iGEN\text{-}ICE}$. Due to the high GEN nominal torque, the ICE start conditions (65)÷(67) and (92)÷(93) are met.

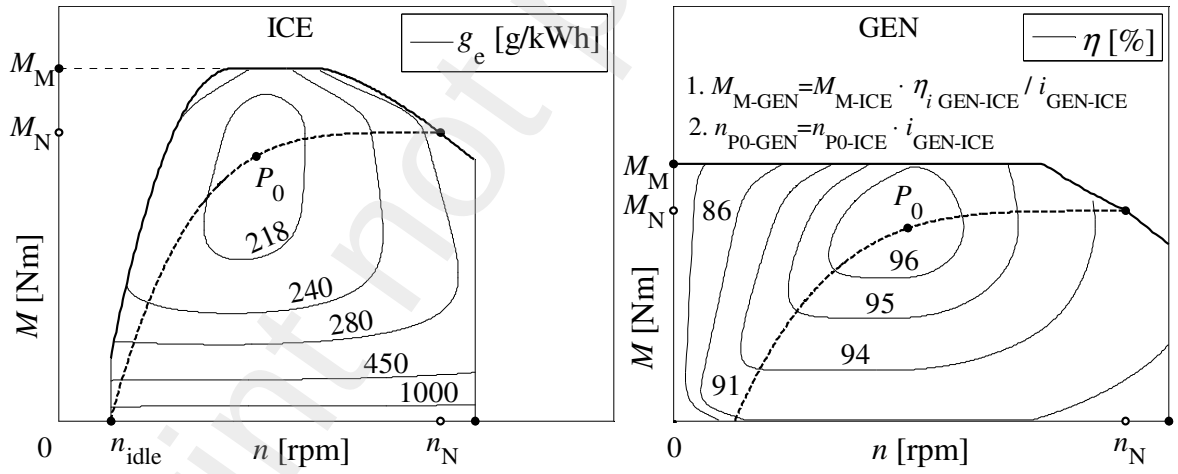

Fig. 18. Matching GEN with ICE.

The total ratio for the EM, based on its maximum speed n_{max_EM}, is the following:

$$i_{EM} = \frac{R_d \cdot n_{max\_EM}}{2.653 \cdot v_{max}} \tag{140}$$

To meet the condition of an uphill start, the EM nominal torque equals:

$$M_{M\_EM} > 3.4 \cdot \frac{m_{gross} \cdot R_d}{i_{EM} \cdot \eta_{tr}} \tag{141}$$

Then, the nominal power of the EM is calculated:

$$N_{N\_EM} = \left(N_{BAT\_Cint} + N_{N\_GEN} \cdot \eta_{INV\_GEN}\right) \cdot \eta_{INV\_EM} \cdot \eta_{EM} \tag{142}$$

This allows a n_{Mmax} point to be determined (68).

10.5. Series-parallel full hybrid drivetrain

The last design is a series-parallel hybrid, also called a power-split hybrid, that uses a planetary gear set to realize the e-CVT presented in Fig. 19.

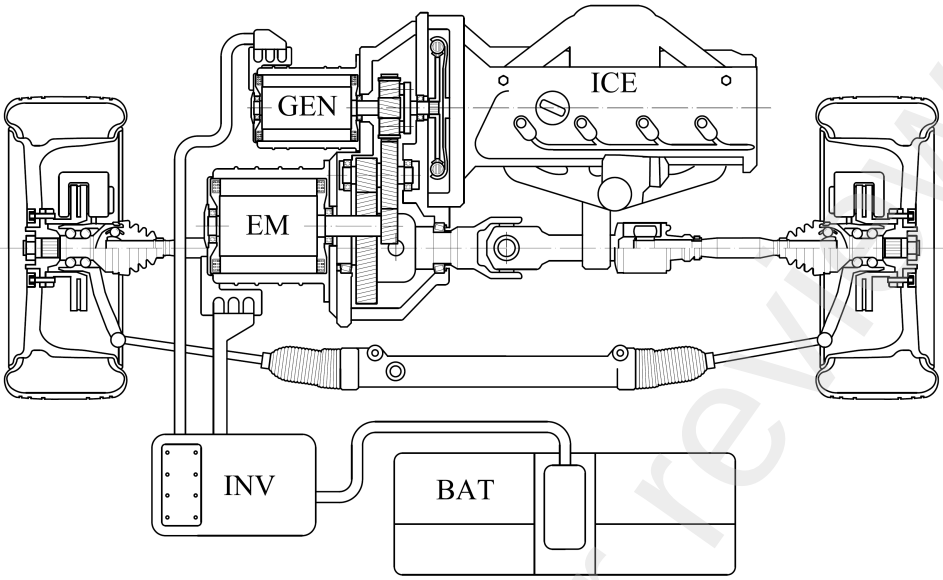

Fig. 19. Series-parallel hybrid drivetrain.

The planetary gear, the main component of such a drivetrain, sometimes called a power-split device (PSD), which connects the ICE, traction EM and GEN, is presented in detail in Fig. 20. Rotational speeds in a PSD are:

$$n_{\mathrm{C}} = n_{\mathrm{R}} \cdot \frac{R_{\mathrm{R}}}{R_{\mathrm{R}} + R_{\mathrm{S}}} + n_{\mathrm{S}} \cdot \frac{R_{\mathrm{S}}}{R_{\mathrm{R}} + R_{\mathrm{S}}} \tag{143}$$

And the relationships between torques are:

$$M_{\mathrm{S}} = M_{\mathrm{C}} \cdot \frac{R_{\mathrm{S}}}{R_{\mathrm{R}} + R_{\mathrm{S}}} \tag{144}$$

$$M_{\mathrm{R}} = M_{\mathrm{C}} \cdot \frac{R_{\mathrm{R}}}{R_{\mathrm{R}} + R_{\mathrm{S}}} \tag{145}$$

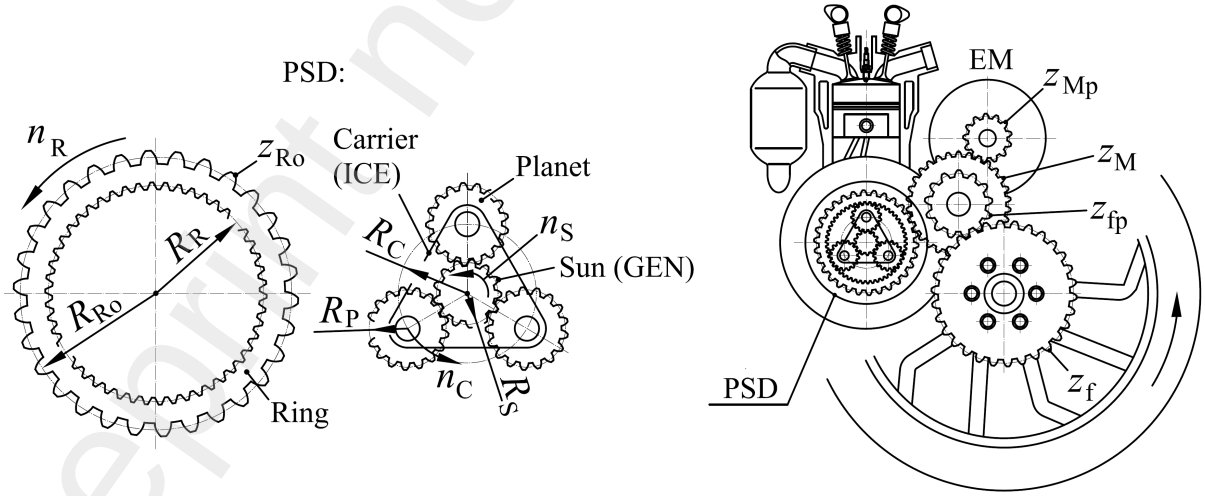

Fig. 20. Power split device in a series-parallel hybrid drivetrain.

All elements of this drivetrain are permanently meshed (no clutches or synchronizers), which results in its high durability.

The EM is permanently connected to the driven wheels by a dual stage, one-speed reduction gear i_{EM}, thus for the maximum vehicle speed v_{max} the following condition is met:

$$i_{EM} = i_M \cdot i_f = \frac{z_M}{z_{Mp}} \cdot \frac{z_f}{z_{fp}} = \frac{R_d \cdot n_{max\_EM}}{2.653 \cdot v_{max}} \tag{146}$$

To design the smallest dual stage reduction gear, the following condition is suggested:

$$\frac{z_M}{z_{Mp}} = \frac{z_f}{z_{fp}} = \sqrt{i_{EM}} \tag{147}$$

The gear ratio $z_M/z_{Ro} \approx 1.000$. Then the ratio of the PSD is determined (Fig. 21). Considering the minimum number of teeth, durability and size conditions, the ratio of the PSD may vary within the range: $i_{PSD} \approx (2.000 \div 4.000)$.

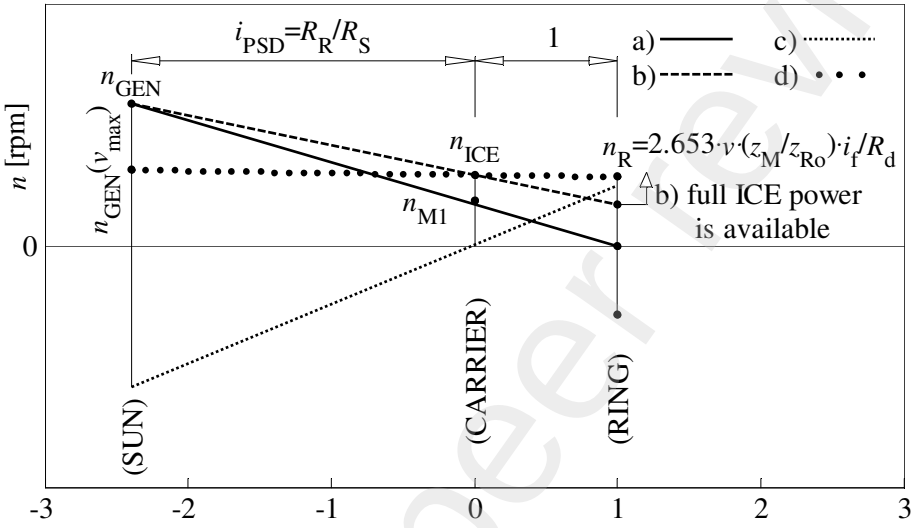

Fig. 21. Conditions determining PSD geometry.

The first condition (Fig. 21 - a) concerns a full-throttle start from a standstill. The GEN reaches its maximum speed n_{GEN_max}, at the same time the ICE should develop its nominal torque M_M, which is reached at $>0.9 \cdot n_{M1}$, to develop the maximum driving force. The ring speed at vehicle start is $n_R=0$. The formula below, based on (143), determines the maximum ratio of a PSD:

$$i_{PSD} \le \frac{n_{max\_GEN}}{0.9 \cdot n_{M1\_ICE}} - 1 \tag{148}$$

The second condition (Fig. 21 – b) concerns the vehicle speed when the ICE reaches n_N. The PSD should have a ratio that prevents the ICE from spinning too fast at a city speed, which lowers the ICE noise. However, the maximum power should be available in the extra urban traffic where the vehicle speed $v_{EU}>90 \div 100$ km/h. This results in:

$$i_{PSD} \ge \frac{n_{max\_GEN} - n_{N\_ICE}}{n_{N\_ICE} - 2.653 \cdot v_{EU} \cdot i_f \cdot z_M / (R_d \cdot z_{Ro})} \tag{149}$$

The third condition (Fig. 21 – c) refers to the maximum speed in the EV mode. In this case, the ICE is off, the carrier is stationary, the GEN reaches its maximum speed (in negative direction), and the PSD ratio is:

$$i_{PSD} \le \frac{\left| n_{max\_GEN} \right|}{2.653 \cdot v_{max\_EV} \cdot i_f \cdot z_M / (R_d \cdot z_{Ro})} \tag{150}$$

The fourth condition (Fig. 21 – d) verifies n_{GEN} at v_{max}. In this case, n_{GEN} must be positive:

$$n_{GEN}(v_{max}) = n_{N\_ICE} \cdot (i_{PSD} + 1) - 2.653 \cdot v_{max} \cdot i_f \cdot (z_M / z_{Ro}) \cdot i_{PSD} / R_d > 0 \tag{151}$$

If this condition is not met, i_f and/or z_M/z_{Ro} should be decreased.

When the geometry of a planetary gear is already set, one can determine the nominal torque of the EM. Uphill driving forward on a slope of 26% (Section 9.1) can be realized with the EM and support from the ICE, which results in:

$$M_{\mathrm{M\_EM}} \geq \frac{3.4 \cdot m_{\mathrm{gross}} \cdot R_{\mathrm{d}} - M_{\mathrm{M\_ICE}} \cdot \left[i_{\mathrm{PSD}} / (i_{\mathrm{PSD}} + 1) \right] \cdot (z_{\mathrm{M}} / z_{\mathrm{Ro}}) \cdot i_{\mathrm{f}} \cdot \eta_{\mathrm{tr\_1}}}{i_{\mathrm{EM}} \cdot \eta_{\mathrm{tr\_2}}} \tag{152}$$

where $\eta_{\mathrm{tr\_1}}$ is the efficiency of all mechanical components from the ICE to the gearwheel z_{M} and $\eta_{\mathrm{tr\_2}}$ is the efficiency of all mechanical components from the EM to the wheels.

However, reverse driving is realized only with the EM, and the results obtained with formula (152) will not allow driving in reverse on a 26% slope. Considering that such a situation has a very small probability of occurrence, only a slope of 15% (which is much more common) must be overcame both in forward and in reverse, which results from (1)÷(8):

$$M_{\mathrm{M\_EM}} \geq 2.4 \cdot \frac{m_{\mathrm{gross}} \cdot R_{\mathrm{d}}}{i_{\mathrm{EM}} \cdot \eta_{\mathrm{tr}}} \tag{153}$$

Then, the GEN parameters are determined. Based on Fig. 21-a, it can be noticed that at $n_{\mathrm{N\_GEN}}$ its torque $M_{\mathrm{N\_GEN}}$ must equal the ICE torque $M_{\mathrm{M\_ICE}}$ multiplied by the PSD ratio:

$$M_{\mathrm{N\_GEN}} = M_{\mathrm{M\_ICE}} \cdot \frac{\eta_{\mathrm{PSD}}}{1 + i_{\mathrm{PSD}}} \tag{154}$$

The nominal generator power $N_{\mathrm{N\_GEN}}$ is:

$$N_{\mathrm{N\_GEN}} = \frac{M_{\mathrm{N\_GEN}} \cdot n_{\mathrm{N\_GEN}}}{9550} \tag{155}$$

These are static parameters for stable working conditions. However, the GEN works frequently in strongly dynamic states, e.g. at ICE start-up the GEN must overcome its inertia and the resistances of the ICE: inertia (40) and internal friction (65). In such a state, the GEN angular acceleration might reach over 1000 rad/s^2. Thus the GEN nominal torque $M_{\mathrm{M\_GEN}}$ is:

$$M_{\mathrm{M\_GEN}} = M_{\mathrm{EM\_start}} + M_{\mathrm{ICE\_start}} \cdot \frac{\eta_{\mathrm{PSD}}}{1 + i_{\mathrm{PSD}}} > M_{\mathrm{N\_GEN}} \tag{156}$$

Then the rated speed n_{Mmax} for the GEN is calculated. When the geometry of a PSD and the GEN parameters are determined, then the N_{EM} and its n_{Mmax} are calculated.

11. Summary

Modelling of a hybrid drivetrain is a process which can initially estimate the considered drivetrain design in the aspect of overall fuel economy, as well as ergonomics and dynamics. To obtain results with high relevance to real constructions, mathematical models of drivetrain components must be prepared with high accuracy. The article delivers a design tool including all the characteristics that allow a hybrid drivetrain to be modelled from scratch, only with basic assumptions required. All necessary characteristics, formulas and tables with relevant coefficients that allow a mild-hybrid or full-hybrid drivetrain to be fully designed are provided. The great advantage is that these characteristics include the warm-up behaviour of the ICE and BAT, which have a significant impact on fuel consumption, especially on short distances. The included simulation of ICE warm-up of BAT thermal behaviour shows a high level of correlation with real constructions.

The design process can be divided into two stages. The first one concerns the uphill condition, maximum speed, and gear ratio selection, resulting from physical phenomena. They refer not only to the designs presented in the article but also to other designs, e.g. Renault E-Tech Hybrid, Suzuki Strong Hybrid or in other DHTs (dedicated hybrid transmissions).

The second stage concerns ergonomics, driver behaviour, and traffic conditions (based on a given homologation test) and can vary with regard to the country, group of countries or continent. Then a proper solution is selected with affordable ranges of parameters.

The proposed characteristics with recommended ranges of parameters are valid for any hybrid drivetrain based on SI ICEs and lithium-ion BATs, which, considering current trends in automotive engineering, will be the main stream for the nearest years. The provided formulas can be implemented in any program, because they are developed as 'ready-to-use', thus they can be useful for students, scientists, engineers as well as enthusiasts in this area searching for more technical information on hybrids.

The presented models are created on average constructions. The aspects common in the case of every hybrid drivetrain were taken into account. However, due to complex control strategies concerning fuel spray in the cylinder or exhaust gases after treatment systems, the NO_x, CO and PM emissions were not considered. In a real system design, where advanced measurement data concerning the ICE and after-treatment system is available, this aspect would also be taken into consideration.

Declarations

Competing interests

There are no competing interests concerning this article.

Funding

This work was supported by the AGH University of Science and Technology, Faculty of Mechanical Engineering and Robotics [Research program No. 16.16.130.942].

References

[1] P. Bielaczyc, J. Woodburn, A. Szczotka, An assessment of regulated emissions and CO_2 emissions from a European light-duty CNG-fueled vehicle in the context of Euro 6 emissions regulations, Applied Energy, 117 (2014), pp. 134–141, doi: http://dx.doi.org/10.1016/j.apenergy.2013.12.003.

[2] P. Bielaczyc, J. Woodburn, A. A. Joshi, World-wide trends in powertrain system development in light of emissions legislation, fuels, lubricants and test methods, Combustion Engines, 184(1) (2021), pp. 57-71, doi: https://doi.org/10.19206/CE-134785.

[3] ACEA Position Paper, Views on proposals for Euro 7 emission standard, December 2020, European Automobile Manufacturers Association.

[4] ICCT's comments and technical recommendations on future Euro 7 emission standards, The International Council of Clean Transportation, Berlin, May 7 2021.

[5] D. Carney, Toyota unveils more new gasoline ICEs with 40% thermal efficiency, 2018-04-04, SAE International.

[6] V.W. Wong, S. C. Tung, Overview of automotive engine friction and reduction trends–
effects of surface, material, and lubricant-additive technologies, Friction, 4(1) (2016), ISSN: 2223-7690, doi: 10.1007/s40544-016-0107-9 CN 10-1237/TH.

[7] H. Ding, et al., Configuration Synthesis and Performance Analysis of 9-Speed Automatic Transmissions, Chinese Journal of Mechanical Engineering, 2020, doi: https://doi.org/10.1186/s10033-020-00466-y.

[8] P. Yadav, et al., Review on weight reduction in automobile, International Journal of Advanced Technology in Engineering and Science, Vol. 4, Issue 01, January 2016, ISSN: 2348-7550.

[9] A. N. M. M. I. Mukut, M. Z. Abedin, Review on aerodynamics drag reduction of vehicles, International Journal of Engineering Materials and Manufacture, 4(1) (2019), pp. 1-14, doi: https://doi.org/10.26776/ijemm.04.01.2019.01.

[10] J. A. Sanguesa, et al., A review on electric vehicles: technologies and challenges, Smart Cities, 4 (2021), pp. 372–404, doi: https://doi.org/10.3390/smartcities4010022.

[11] D. Pevec, J. Babic, A. Carvalho, Electric Vehicle Range Anxiety: An obstacle for the personal transportation (r)evolution?, IEEE Xplore, 2019 4th International Conference on Smart and Sustainable Technologies (SpliTech), doi: 10.23919/SpliTech.2019.8783178.

[12] J. J. Gómez Vilchez, et al., Electric car purchase price as a factor determining consumers' choice and their views on incentives in Europe, Sustainability, 11 (2019), doi:10.3390/su11226357.

[13] S. Ma, et al.: Temperature effect and thermal impact in lithium-ion batteries: A review, Progress in Natural Science: Materials International, 28 (2018), pp. 653–666, doi: https://doi.org/10.1016/j.pnsc.2018.11.002.

[14] V. Ruiz, Standards for the performance and durability assessment of electric vehicle batteries, EUR 29371 EN, Publications Office of the European Union, Luxembourg, 2018, ISBN 978-92-79-94179-5, doi:10.2760/24743, JRC113420.
[15] N. Haque, A. Hughes, S. Lim, C. Vernon, Rare Earth Elements: Overview of Mining, Mineralogy, Uses, Sustainability and Environmental Impact, Resources, 3 (2014), pp. 614-635; doi:10.3390/resources3040614.
[16] Y. Wang, et al., The impact of electric vehicle charging on grid reliability, IOP Conf. Ser.: Earth Environ. Sci. 199 052033, 2018, doi:10.1088/1755-1315/199/5/052033.
[17] U. Asif, K. Schmidt, Fuel Cell Electric Vehicles (FCEV): Policy Advances to Enhance Commercial Success, Sustainability, 13 (2021), 5149, doi: https://doi.org/10.3390/su13095149.
[18] C. Yi, et al., Modeling, control, and performance of a novel architecture of hybrid electric powertrain system, Applied Energy, 178 (2016), pp. 454–467, doi: http://dx.doi.org/10.1016/j.apenergy.2016.06.068.
[19] H. Peng, et al., Synthesis and analysis method for powertrain configuration of single motor hybrid electric vehicle, Mechanism and Machine Theory, 146 (2020), 103731, doi: https://doi.org/10.1016/j.mechmachtheory.2019.103731.
[20] W. Zhuang, et al., A survey of powertrain configuration studies on hybrid electric vehicles, Applied Energy, 262 (2020), 114553, doi: https://doi.org/10.1016/j.apenergy.2020.114553.
[21] Z. Lei, et al., Analysis and coordinated control of mode transition and shifting for a full hybrid electric vehicle based on dual clutch transmissions, Mechanism and Machine Theory, 114 (2017), pp. 125–140, doi: http://dx.doi.org/10.1016/j.mechmachtheory.2017.04.001.
[22] P. Bera, W. Sikora, D. Wędrychowicz, Non-linear control of a gear shift process in a dual-clutch transmission based on a neural engine model, Control Engineering Practice, 115 (2021), 104886, doi: https://doi.org/10.1016/j.conengprac.2021.104886.
[23] I. Pielecha, W. Cieslik, K. Fluder, Analysis of energy management strategies for hybrid electric vehicles in urban driving conditions, Combustion Engines, 173(2) (2018), pp. 14-18, doi: 10.19206/CE-2018-203.
[24] H. Wang, X. Zhang, M. Ouyang, Energy consumption of electric vehicles based on real-world driving patterns: A case study of Beijing, Applied Energy, 157 (2015), pp. 710–719, doi: http://dx.doi.org/10.1016/j.apenergy.2015.05.057.
[25] J. Kleiner, et al., Thermal Modelling of a Prismatic Lithium-Ion Cell in a Battery Electric Vehicle Environment: Influences of the Experimental Validation Setup, Energies, 2020, 13, 62, doi:10.3390/en13010062.
[26] A. M. Aris, B. Shabani, An experimental study of a lithium ion cell operation at low temperature conditions, Energy Procedia, 110 (2017), pp. 128 – 135, doi: 10.1016/j.egypro.2017.03.117.
[27] A. H. Mahmud, Z. H. C. Daud, Z. Asus, The impact of battery operating temperature and state of charge on the lithium-ion battery internal resistance, Jurnal Mekanikal, Vol. 40, June 2017, pp. 01-08.
[28] D. Wang, Y. Bao, J. Shi, Online Lithium-Ion Battery Internal Resistance Measurement Application in State-of-Charge Estimation Using the Extended Kalman Filter, Energies, 2017, 10, 1284, doi:10.3390/en10091284.
[29] C. Capasso, O. Veneri, Experimental analysis on the performance of lithium based batteries for road full electric and hybrid vehicles, Applied Energy, 136 (2014), pp. 921–930, doi: http://dx.doi.org/10.1016/j.apenergy.2014.04.013.
[30] M. Ehsani, et al., Modern electric, hybrid electric, and fuel cell vehicles: fundamentals, theory and design, CRC Press, Boca Raton, 2005, ISBN: 0-8493-3154-4.
[31] G. Lechner, H. Naunheimer, Automotive transmissions: Fundamentals, selection, design and application, Springer-Verlag Berlin Heidelberger, Germany, 1999, ISBN: 3-540-65903-X.
[32] W. Siłka, Theory of vehicle motion (translated from Polish), WNT, Warsaw, 2002, ISBN: 83-204-2748-7.
[33] D. Crolla, et al., Encyclopedia of automotive engineering, John Wiley & Sons, 2015, pp. 886-887, ISBN: 978-0-470-97402-5.
[34] I. Husain, Electric and hybrid vehicles, design fundamentals, CRC Press, Taylor&Francis Group, ISBN: 978-1-138-59058-8.
[35] J. A. Wajand, J. T. Wajand, Reciprocating combustion engines (translated from Polish), Warszawa, 2005, Wydawnictwa Naukowo-Techniczne, ISBN: 83-204-3054-2.

[36] P. Bera, Torque characteristic of SI engine in dynamic operating states, Combustion Engines, 171 (2017), pp. 175-180, doi: https://doi.org/10.19206/CE-2017-429.
[37] P. Bera, 2019, Development of engine efficiency characteristic in dynamic working states, Energies, 12, 2906, doi: https://doi.org/10.3390/en12152906.
[38] A. Czerwonka, Internal combustion engine inertia as a factor limiting vehicle dynamics, Engineering thesis, AGH University of Science and Technology, 2021.
[39] A. Ubysz, Problems of rotational mass in passenger vehicles, Transport Problems, 2010, Volume 5, Issue 1.
[40] J. B. Heywood, Internal Combustion Engine Fundamentals, McGaw-Hill, Inc., United States of America, 1988, ISBN: 0-07-028637-X.
[41] M. Razmara, et al., Optimal exergy-based control of internal combustion engines, Applied Energy, 183 (2016), pp. 1389–1403, doi: http://dx.doi.org/10.1016/j.apenergy.2016.09.058.
[42] A. Roberts, R. Brooks, P. Shipway, Internal combustion engine cold-start efficiency: A review of the problem, causes and potential solutions, Energy Conversion and Management, 82 (2014), pp. 327–350, doi: http://dx.doi.org/10.1016/j.enconman.2014.03.002.
[43] R. Cipollonea, D. Di Battista, M. Maurielloa, Effects of oil warm up acceleration on the fuel consumption of reciprocating internal combustion engines, Energy Procedia, 82 (2015), pp. 1 – 8, doi: 10.1016/j.egypro.2015.11.870.
[44] J. D. Trapy, P. Damiral, An investigation of lubricating system warm-up for the improvement of cold start efficiency and emissions of S.I. automotive engines, SAE Transactions, 1990, Vol. 99, Section 6: Journal of passenger cars, 1990, pp. 1635-1645, SAE International.
[45] D. Di Battista, R. Cipollone, Experimental and numerical assessment of methods to reduce warm up time of engine lubricant oil, Applied Energy, 162 (2016), pp. 570–580, doi: http://dx.doi.org/10.1016/j.apenergy.2015.10.127.
[46] B. Derbiszewski, et al., A study on the flow resistance of fluids flowing in the engine oil-cooler chosen, Lubricants, 2021, 9, 75, doi: https://doi.org/10.3390/lubricants9080075.
[47] K. PáV, V. Rychtář, V. Vorel, Heat balance in modern automotive engines, Škoda Auto a.s., Mladá Boleslav 293 60, Mecca 02 2012, doi: 10.2478/v10138-012-0007-7.
[48] M. Rundo, N. Nervegna, Lubrication pumps for internal combustion engines: a review, International Journal of Fluid Power, Vol. 16, No. 2, 2015, pp. 59–74, doi: http://dx.doi.org/10.1080/14399776.2015.1050935.
[49] F. Liu, Analysis of BJ493 diesel engine lubrication system properties, IOP Conf. Series: Materials Science and Engineering, 283 (2017), 012005, doi:10.1088/1757-899X/283/1/012005.
[50] Oil pumps for internal combustion engines and transmissions. Conventional, Variable and Electrical, Pierburg pump technology GmbH, 2012, Alfred Pierburg StraBe, 41460 Neuss, Germany.
[51] Temperature-controlled lubricating oil pumps save fuel, 7th LuK Symposium, 11/12 April 2002, LuK GmbH & Co, Industriestrasse 3, D-77815 Buhl/Baden.
[52] R. Rahmani, et al., The effect of cylinder liner operating temperature on frictional loss and engine emissions in piston ring conjunction, Applied Energy, 191 (2017), pp. 568–581, doi: http://dx.doi.org/10.1016/j.apenergy.2017.01.098.
[53] A. Shimada, et al., An Analysis of Oil Film Temperature, Oil Film Thickness and Heat Transfer on a Piston Ring of Internal Combustion Engine: The Effect of Local Lubricant Viscosity, SAE 2004-32-0024, JSAE 20044311.
[54] P. G. Nikolakopoulos, et al., Lubrication performance of engine commercial oils with different performance levels: The effect of engine synthetic oil aging on piston ring tribology under real engine conditions, Lubricants 2018, 6, 90, doi:10.3390/lubricants6040090.
[55] S. Sun, N. Sun, X. Wang, Study on mixed lubrication characteristics of piston/cylinder interface of variable length, AIP Advances, 9, 075303 (2019), doi: https://doi.org/10.1063/1.5093925.
[56] Z. Žák, et al., In-cylinder heat transfer modelling, Mecca, 03 2016, De Gruyter Open, doi: 10.1515/mecdc-2016-0009.
[57] D. Sandoval, J. B. Heywood, An improved friction model for spark-ignition engines, SAE International, 2003, doi: https://doi.org/10.4271/2003-01-0725.
[58] R. S. Jeffrey, Characterization and modeling of rubbing friction in a motored four-cylinder internal combustion engine, Master's Thesis of Applied Science in the Department of Mechanical Engineering, McMaster University, Hamilton, Canada, 2011.

[59] Mobil Super™ Synthetic, Mobil Passenger Vehicle Lube, Exxon Mobil Corporation, 22777 Springwoods Village Parkway, Spring TX 77389.
[60] J. Pavlovic, A. Marotta, B. Ciuffo, CO_2 emissions and energy demands of vehicles tested under the NEDC and the new WLTP type approval test procedures, Applied Energy, 177 (2016), pp. 661–670, doi: http://dx.doi.org/10.1016/j.apenergy.2016.05.110.
[61] P. Dong, et al., Coordinated clutch slip control for the engine start of vehicles with P2-hybrid automatic transmissions, Mechanism and Machine Theory, 153 (2020), 103899, doi: https://doi.org/10.1016/j.mechmachtheory.2020.103899.
[62] K. D. Huang a, S.-C. Tzeng, A new parallel-type hybrid electric-vehicle, Applied Energy, 79 (2004), pp. 51–64, doi:10.1016/j.apenergy.2003.12.001.
[63] A. Emadi, Advanced electric drive vehicles, CRC Press, Taylor&Francis, 2014, ISBN: 978-1-4665-9770-9.
[64] H. Maleki, et al., Thermal Properties of Lithium-Ion Battery and Components, Journal of The Electrochemical Society, 146 (3) (1999), pp. 947-954, doi: 10.1149/1.1391704.
[65] Z. Wang, J. Ma, L. Zhang, Finite Element Thermal Model and Simulation for a Cylindrical Li-Ion Battery, China National Engineering Laboratory for Electric Vehicles, Beijing Institute of Technology, Beijing 100081, China, 2017, doi: 10.1109/ACCESS.2017.2723436.
[66] D. Chen, et al., Comparison of different cooling methods for lithium ion battery cells, Applied Thermal Engineering, 94 (2016), pp. 846–854, doi: http://dx.doi.org/10.1016/j.applthermaleng.2015.10.015.
[67] P. G. Anselma, Battery state-of-health sensitive energy management of hybrid electric vehicles: Lifetime prediction and ageing experimental validation, Applied Energy, 285 (2021), 116440, doi: https://doi.org/10.1016/j.apenergy.2021.116440.
[68] P. Drage, et al., Cabin conditioning for electric vehicles, ATZ worldwide, 02/2019.
[69] R. Groiß, The influence of temperature on the operation of batteries and other electrochemical energy storage systems, BaSyTec GmbH, Öllinger Weg 17, 89176 Asselfingen, Germany, 2018.
[70] P. Bera, A design method of selecting gear ratios in manual transmissions of modern passenger cars, Mechanism and Machine Theory, 132 (2019), pp. 133–153, doi: https://doi.org/10.1016/j.mechmachtheory.2018.10.013.
[71] Y. Chem, Automotive transmissions. Design Theory and applications, Springer, 2021, ISBN: 978-981-15-6702-5, doi: https://doi.org/10.1007/978-981-16-6703-2.
[72] A. H. Kotarba, Determination of the influence of car wheels inertia on vehicle dynamics, Engineering thesis, AGH University of Science and Technology, 2021.
[73] P. R. Kowalski, Determination of the inertia influence of the drivetrain elements on vehicle dynamics, Engineering thesis, AGH University of Science and Technology, 2021.
[74] Z. Jaśkiewicz, Calculations of Drivetrains (Translated from Polish), WKiŁ, Warsaw, 1972, ISBN: 83-7207-313-9.
[75] Freons Sauleda, Automotive clutch facings, Material G95, E-08396 Sant Cebrià de Vallalta, Barcelona, Spain.
[76] J. Javorski Eckert, et al., Vehicle drivetrain design multi-objective optimization, Mechanism and Machine Theory, 156 (2021), 104123, doi: https://doi.org/10.1016/j.mechmachtheory.2020.104123.
[77] R. Stopp, C. Siefert, 7th LuK Symposium, 11/12.04.2002, Germany, GMBH, LuK Symposium.
[78] R. P. Willems, Longitudinal Behavior Planning with Maneuver Prediction for Urban Driving, Master of science thesis, Delft University of Technology, 2018.
[79] I. Bae, J. Moon, J. Seo, Toward a Comfortable Driving Experience for a Self-Driving Shuttle Bus, Electronics, 2019, 8(9), 943, doi:10.3390/electronics8090943.
[80] Y. You, D. Sun, D. Qin, Research on vehicle starting control based on reflux power condition, Mechanism and Machine Theory, 134 (2019), pp. 289–307, doi: https://doi.org/10.1016/j.mechmachtheory.2019.01.003.

Nomenclature and units:

a_v	Vehicle acceleration [m/s^2]
A	Vehicle frontal area [m^2]
C_d	Aerodynamic drag coefficient [-]
F	Force [N]
g	Gravity constant [9.81 m/s^2]
g_e	Brake specific fuel consumption (*bsfc*) [g/kWh]
H	Heat flow [W]
i	Gear ratio [-]
J	Moment of inertia [kgm^2]
m	Mass [kg]
M	Torque [Nm]
n	Rotational speed [rpm]
N	Power [kW]
R_d	Driven wheel dynamic radius [m]
t	Time [s]
$temp$	Temperature [^{o}C]
v	Vehicle speed [km/h]
V_{ICE}	ICE displacement [dm^3]
ε	Angular acceleration [rad/s^2]
η	Efficiency [%]
ν	Kinematic viscosity [mm^2/s]
ρ_{air}	Ambient air density [1.21 kg/m^3]
ρ_{fuel}	Petrol density [0.75 g/cm^3]